Analytical Volterra-based models for nonlinear low order flight dynamics approximation systems

A. Omran
CNH-Fiat Industrial
Burr-Ridge, Illinois
USA

B. Newman
Dept of Mechanical and Aerospace Engineering
Old Dominion University
Norfolk, Virginia
USA

ABSTRACT

Analytical methodology is presented to conduct dynamical assembly of simple low order nonlinear responses for system synthesis and prediction using Volterra theory. The procedure is set forth generically and then applied to several atmospheric flight examples. A two-term truncated Volterra series, which is enough to capture the quadratic and bilinear nonlinearities, is developed for first and second order generalised nonlinear single degree of freedom systems. The resultant models are given in the form of first and second kernels. A parametric study of the influence of each linear and nonlinear term on kernel structures is investigated. A step input is then employed to quantify and qualify the nonlinear response characteristics. Uniaxial surge and pitch motions are presented as examples of the low order flight dynamic systems. These examples show the ability of the proposed analytical Volterra-based models to predict, understand, and analyse the nonlinear aircraft behaviour beyond that attainable by linear-based models. The proposed analytical Volterra-based model offers an efficient nonlinear preliminary design tool in qualifying the aircraft responses before computer simulation is available or invoked.

Paper No. 3730. Manuscript received 10 June 2011, revised version received 13 December 2011, accepted 15 March 2012.

https://doi.org/10.1017/S0001924000007533 Published online by Cambridge University Press

NOMENCLATURE

a	time constant of the first order system
$\bar{c}$	wing mean aerodynamic chord, ft
C_L	lift coefficient
C_D	drag coefficient
C_m	pitching moment coefficient
g	acceleration due to gravity
h_k	Volterra kernel of kth order
H	altitude
H_e	engine angular momentum
I_X	moment of inertia about X axis
I_Y	moment of inertia about Y axis
I_Z	moment of inertia about Z axis
I_{XZ}	product of inertia with respect to X and Z body axes
m	airplane mass
p	airplane roll rate
q	airplane pitch rate
$\bar{q}$	dynamic pressure
r	airplane yaw rate
S	reference area
t	time
T	total instantaneous engine thrust
u	velocity components in X axis or input vector
v	velocity components in Y axis
V	aircraft total velocity
w	velocity components in Z axis
$\mathbf{x}$	state vector
$\mathbf{y}$	output vector
α	angle-of-attack
β	sideslip angle
δ_e	elevator deflection
δ_a	aileron deflection
δ_t	throttle deflection
σ	damping factor
φ	roll angle
θ	pitch angle
ψ	yaw angle
γ	flight path angle
ω_d	damped ad undamped natural frequency
ω_n	undamped natural frequency
τ	time
ζ	damping ratio

Other terms are defined where they first appear in the text. Having regard to the historical viewpoint and consistency with quotations, contemporary terminology and units are used throughout. Units were mostly based on the pound-foot-second system.

https://doi.org/10.1017/S0001924000007533 Published online by Cambridge University Press

1.0 INTRODUCTION

For various types of aircraft, many nonlinear phenomena such as pitch-up, stall, elevator or rudder control surface blockage, wing rock, roll-yaw spin inertial coupling, nose slice, falling leaf, and pilot-induced oscillation have been observed during unusual attitudes and extreme maneuvers. These phenomena are consequences of system nonlinearities including but not limited to nonlinear aerodynamics, moments of inertia characteristics, and actuator limits. Characterising and analysing aircraft dynamic behaviour to expose mechanisms underlying these phenomena based on nonlinear simulation is a prohibitive task since tracing the behaviour characteristics back to their nonlinear parametric origins based on numeric propagation is virtually impossible. For that reason, a relational procedure is developed in this paper that addresses these casual model nonlinearities and control effects on the system nonlinear responses. The essence of many nonlinear dynamic behaviour in multi-axis aircraft motion can be rendered with simple first order and second order single degree-of-freedom (SDOF) submodels, and this paper places emphasis on these simplified model structures. The motion response is presented as a set of kernels, where each kernel carries the system's linear and/or nonlinear information. Parametric study of the influence of each term on the overall kernel structures is then conducted for qualitative and quantitative analyses. The purpose of this parametric study is to explore a methodology whereby dynamical assembly of the system's nonlinear behaviour can be better understood.

Constructing an analytical model describing nonlinear aircraft dynamic behaviour has been investigated using various approximation techniques. Three common approaches appear in the literature to predict nonlinear phenomena: bifurcation approach[1-9], describing function approach[10-13] and perturbation and time scale approaches[14-18]. Bifurcation analysis has been applied to many nonlinear phenomena such as wing rock[1-5], spin entry[5-8] and pilot-induced oscillation[9]. Describing function analysis has been used mostly to generate limit-cycle behaviour in many flight dynamic models as reported in Refs 10-13. Since perturbation expansion analysis breaks down quickly in time or in parameter strength, the technique has rarely been applied in flight mechanics research. One example is given in Ref. 14. Although all these techniques show potential to understand and analyse nonlinear behaviour of aircraft, these methods sometimes do not provide a precise cause-and-effect result, do not address transient behaviour, or do not cover a sufficient range of time and/or parameter variation. In fact, none of these techniques has the capability to construct a general conclusion for the nonlinearity consequences, because of the iterative and computational details in developing these models, which restrict any general symbolic development to nonlinear systems. This concludes that there is a need to more structural nonlinear approximation method, which has the same capability as the linear theory. Volterra theory has the seeking structure, which is presented by the so-called 'Volterra kernels'.

Volterra theory has emerged as a popular nonlinear modeling technique, primarily because of the underlying analytical framework and its extension of the impulse response concept from linear theory. Volterra theory dates back to 1887 with the first encompassing publication appearing in 1927 and later in 1958[19-20]. An early use of this theory was made by Wiener and subsequent research was conducted at the Massachusetts Institute of Technology in the area of filtering and electronic circuits [21-23]. Few applications of the Volterra methodology to flight mechanics appear in the literature. References 24-25 are two notable exceptions. In these efforts, modelling the longitudinal dynamics of a high performance aircraft in limit cycling conditions has been explored via the Volterra approach. In Ref. 25, a differential form

https://doi.org/10.1017/S0001924000007533 Published online by Cambridge University Press

of a reduced third order Volterra series was considered. The approach proved the ability to capture the limit cycle. This work was extended in Ref. 24 to a global approach. An interesting application of Volterra theory in flight mechanics is presented in Ref. 26 to analytically define nonlinear flying quality metrics. However, most of these trials date back to the 1980s and early 1990s. Recently, in Refs 27-28, the authors have brought back the utilisation of Volterra theory to flight mechanics through a global piecewise approach. This approach facilitates the use of Volterra theory in a piecewise fashion or a parameter varying fashion for strong nonlinearity. Continuing this effort of utilising Volterra theory in flight mechanics research, a new trial to use the theory in analytically predicting nonlinear behaviour is investigated herein.

This paper presents an analytical framework to predict the nonlinear behaviour of the first and second order SDOF subsystems by dynamical assembly. The work is considered a demonstration tool to understand and analyse the nonlinear phenomena observed in aircraft dynamic behaviour. Symbolic generic nonlinear SDOF first and second order systems are investigated as basic representations for system dynamics. The nonlinearity herein is mathematically considered as state quadratic terms, input quadratic term, and as state/input bilinear terms. A variational expansion methodology, one of the most efficient analytical Volterra techniques, is used to develop an approximate nonlinear solution. The solution is given as a two-term truncated Volterra series. The two terms symbolise the first and second kernels, which is enough to capture the quadratic and bilinear information initially assumed in the nonlinear systems. Such an analytical solution is visualised in the time domain for understanding the influence of each nonlinear/linear term appearing in the kernel structure. Following the same rationale of linear analyses in the literature, a parametric exploration for a nonlinear step response is conducted to characterise the overall system response from the fundamental components. Feasibility of the proposed implementation is assessed in two examples: surge and pitch motions. The approximate response of the Volterra-based models is compared to the linear and nonlinear simulation responses to show the capability of the developed model to predict the nonlinear behaviour of the aircraft.

2.0 LOW ORDER UNIAXIAL FLIGHT DYNAMIC SUBSYSTEMS

This section shows how the full order aircraft dynamic model can be represented as a set of low order flight dynamic subsystems while preserving the link to the more general model. The two low order system examples: surge and pitch motions, are offered herein as demonstrations. Each example represents a SDOF uniaxial motion. Reference 29 contains a frequently cited full order dynamic model of a high performance aircraft. This model is considered under many assumptions: the aircraft is a rigid body with six degrees-of-freedom (6DOF) except for an internal constant spinning engine rotor, the aircraft mass is constant, the aircraft body is symmetric about the *XZ* plane, the atmosphere is stationary, and the earth is flat with constant gravity. Based on those assumptions the nonlinear equations of motion, derived from Newtonian mechanics, are listed in Refs 29-30, which have been omitted from this paper.

The dominant nonlinear behaviour of a conventional aircraft can be fairly well described by a symmetric motion (longitudinal) and an asymmetric motion (lateral-directional). In the

https://doi.org/10.1017/S0001924000007533 Published online by Cambridge University Press

case of symmetric longitudinal flight, the lateral-directional variables are exactly zero due to airplane symmetry about the *XZ* plane. Using the stability axes and the relations $w = V\,\mathrm{Sin}(\alpha)$, $u = V\,\mathrm{Cos}(\alpha)$, and $V^2 = u^2 + w^2$, one can replace the surge u and heave w equations by the total velocity V and the angle-of-attack α equations. A reduced nonlinear longitudinal model can then describe the aircraft motion as:

$$\dot{V} = \frac{\mathrm{Cos}(\alpha)}{m} T(M,H,\delta_{th}) - \frac{\bar{q}S}{m} C_D(\alpha,\delta_e) - g\,\mathrm{Sin}(\theta-\alpha) \quad \ldots (1)$$

$$\dot{\alpha} = q - \frac{\mathrm{Sin}(\alpha)}{mV} T(M,H,\delta_{th}) - \frac{\bar{q}S}{mV} C_L(\alpha,\delta_e) + \frac{g}{V}\mathrm{Cos}(\theta-\alpha) \quad \ldots (2)$$

$$\dot{q} = \frac{\bar{q}S\bar{c}}{I_Y} C_m(\alpha,q,\beta=0,\delta_e) \quad \ldots (3)$$

$$\dot{\theta} = q \quad \ldots (4)$$

where

$$C_D = -C_x\mathrm{Cos}(\alpha) - C_z\mathrm{Sin}(\alpha) \qquad C_L = -C_z\mathrm{Cos}(\alpha) + C_x\sin(\alpha) \quad \ldots (5)$$

If an autopilot is assumed to hold the altitude to a constant value H_o and the flight path angle $\gamma_o = \theta_o - \alpha_o$ at zero value, then the total velocity variation is given as:

$$\dot{V} = \frac{\mathrm{Cos}(\alpha_o)}{m} T(V,H_o,\delta_{th}) - \frac{\rho V^2 S}{2m} C_D(\alpha_o,\delta_{eo}) = f\left(V,\delta_{th},\hat{\theta}\right) \quad \ldots (6)$$

where α_o and δ_{eo} are the trimmed angle-of-attack and elevator deflection, which are determined by the specified parameter vector $\hat{\boldsymbol{\theta}} = [H_o \;\; V_o]^T$. Equation (6) represents a first order SDOF system for total velocity with the throttle deflection as the input. The perturbation form of Equation (6) is given by introducing the derivatives of the function f as:

$$\Delta\dot{V} \approx \frac{\partial f}{\partial V}\left(\hat{\theta}\right)\Delta V + \frac{\partial f}{\partial \delta_{th}}\left(\hat{\theta}\right)\Delta\delta_{th} + \frac{1}{2!}\frac{\partial^2 f}{\partial V^2}\left(\hat{\theta}\right)\Delta V^2 + \frac{\partial^2 f}{\partial V \partial \delta_{th}}\left(\hat{\theta}\right)\Delta V\Delta\delta_{th} + \frac{1}{2!}\;\frac{\partial^2 f}{\partial \delta_{th}^2}\left(\hat{\theta}\right)\Delta\delta_{th}^2 + \cdots \quad \ldots (7)$$

The two perturbed quantities ΔV and $\Delta\delta$th, not necessarily small, are measured from the nominal values defined at the operating condition. Since the aerodynamic and engine models of the aircraft are given in the form of look-up tables, a finite difference technique is the proper choice to compute the derivatives appearing in Equation (7).

Another example of a longitudinal low order flight subsystem is the nonlinear pitching motion. In this pitching motion, the total velocity is assumed constant in magnitude ($V = V_o$) and direction ($\gamma = \gamma_o = 0$, $\theta = \alpha$). The pitch motion is then described by a second order SDOF subsystem as:

$$\begin{aligned} \dot{\theta} &= q \\ \dot{q} &= \frac{\bar{q}S\bar{c}}{I_Y} C_m(\theta,q,\delta_e) = f\left(\theta,q,\delta_e,\hat{\theta}\right) \end{aligned} \quad \ldots (8)$$

https://doi.org/10.1017/S0001924000007533 Published online by Cambridge University Press

The parameter vector $\hat{\theta}$ is introduced through $\bar{q}$. Expanding the nonlinear function f around the nominal point, defined by $\hat{\theta}$, leads to

$$\begin{aligned}
&\Delta\dot{\theta} = \Delta q \\
&\Delta\dot{q} \approx \frac{\partial f}{\partial \theta}\left(\hat{\theta}\right)\Delta\theta + \frac{\partial f}{\partial q}\left(\hat{\theta}\right)\Delta q + \frac{\partial f}{\partial \delta_e}\left(\hat{\theta}\right)\Delta\delta_e + \frac{1}{2!}\frac{\partial^2 f}{\partial \theta^2}\left(\hat{\theta}\right)\Delta\theta^2 + \frac{1}{2!}\frac{\partial^2 f}{\partial q^2}\left(\hat{\theta}\right)\Delta q^2 \\
&\quad + \frac{\partial^2 f}{\partial \theta \partial q}\left(\hat{\theta}\right)\Delta\theta\Delta q + \frac{\partial^2 f}{\partial \theta \partial \delta_e}\left(\hat{\theta}\right)\Delta\theta\Delta\delta_e + \frac{\partial^2 f}{\partial q \partial \delta_e}\left(\hat{\theta}\right)\Delta q\Delta\delta_e + \frac{1}{2!}\frac{\partial^2 f}{\partial \delta_e^2}\left(\hat{\theta}\right)\Delta\delta_e^2 + \cdots
\end{aligned} \quad \ldots (9)$$

The perturbed quantities $\Delta\theta$, Δq and $\Delta\delta_e$ are defined from the nominal value determined by the operating condition $\hat{\theta} = [H_o \;\; V_o]^T$. The two uniaxial flight examples of surge and pitch motions represent the aircraft behaviour as a SDOF first or second order system. In Refs 34-35, the authors developed another two equivalent examples for the lateral motion.

3.0 VOLTERRA THEORY

Many physical systems can be described across a set of nonlinear differential and algebraic equations between the input signal $u \in R^m$, the state signal $x \in R^n$, and the output signal $y \in R^p$, where R^N is the N-dimensional real space. A commonly used representation is the nonlinear state space form

$$\begin{aligned}
\dot{x}(t) &= f\left(t, x(t), u(t)\right) \\
y(t) &= g\left(t, x(t), u(t)\right)
\end{aligned} \quad \ldots (10)$$

Vectors $f \in R^n$ and $g \in R^p$ denote the system nonlinearities and $t \in R^t$ is time. Volterra theory represents the input-output relation of a nonlinear system as an infinite sum of multi-dimensional convolution integrals [20]:

$$y(t) = h_o(t) + \sum_{k=1}^{\infty} \int_0^{\infty}\int_0^{\infty} \cdots \int_0^{\infty} h_k(\tau_1, \tau_2, \ldots, \tau_k) \cdot \prod_{i=1}^{k} u(t-\tau_i)\, d\tau_i \quad \ldots (11)$$

In Equation (11), $h_k(\tau_1,\tau_2,\ldots\tau_k)$ denotes the kth order Volterra kernel. Volterra kernels are causal functions with respect to their argument[20]. For developing analytical Volterra kernels from the nonlinear differential equation, the variational expansion form, also called the differential form, is used. Variational method was initially developed based on a perturbation point of view with the first notable application in Ref. 31 showing the capability to capture the aircraft behaviour in many nonlinear phenomena in Refs 24-28.

Before applying the differential method to the low order flight systems in Section II, the outline of the method for a single input case is first given to show the mechanism by which the analytical kernels can be constructed. The method assumes the state vector derivative $\dot{x}$ is expandable as an infinite power series in terms of the state vector $v \in R^n$ and scalar input $u \in R^i$ around an arbitrary point, defined by (x_o,u_o), as:

$$\dot{x} = f(x,u) = \sum_{i=0}^{\infty}\sum_{j=0}^{\infty} \tilde{K}_{ij} x^{(i)} u^j \qquad x^{(i)} = x\prod_{k=1}^{i-1} \otimes x \quad \text{and} \quad x^{(0)} = 1 \;\; , x^{(1)} = x \quad \ldots (12)$$

In Equation (12), $\otimes$ is the Kronecker product, which sometimes is called direct product or tensor product. The Kronecker product is a common mathematical operator in the control and signal processing to approximate nonlinear functions to a polynomial form. The Kronecker product for

https://doi.org/10.1017/S0001924000007533 Published online by Cambridge University Press

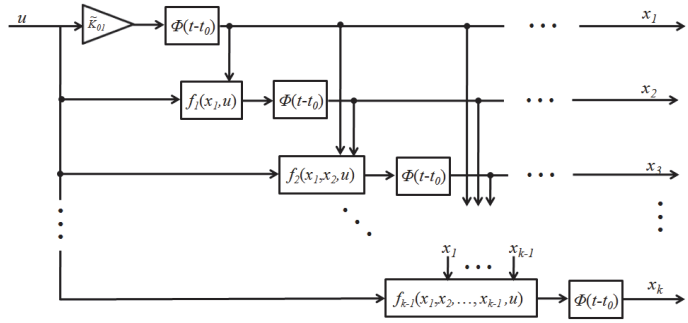


Figure 1. Variational expansion method schematic diagram.

two matrices **P** of dimension $N_P \times M_P$ and Q of dimension $N_Q \times M_Q$ is defined as[20]

$$\mathbf{P} \otimes \mathbf{Q} = \begin{bmatrix} P_{11}Q & \cdots & P_{1M_P}Q \\ \vdots & \ddots & \vdots \\ P_{N_P1}Q & \cdots & P_{N_PM_P}Q \end{bmatrix} \quad \ldots (13)$$

The resultant matrix $\mathbf{P}\otimes\mathbf{Q}$ is of the size (N_PN_Q) (M_PM_Q). The matrix $\tilde{\mathbf{K}}_{\mathbf{ij}}$ of dimension $n \times n_i$ is defined as:

$$\tilde{\mathbf{K}}_{\mathbf{ij}} = \begin{bmatrix} (K_{11})_{ij} & \cdots & (K_{1n^i})_{ij} \\ \vdots & \ddots & \vdots \\ (K_{n1})_{ij} & \cdots & (K_{nn^i})_{ij} \end{bmatrix}, \quad i,j \in \{0,1,2,\cdots,\infty\} \text{ and } \tilde{K}_{00} = 0 \quad \ldots (14)$$

Note $\tilde{K}_{00}$ has a null value. Thus, the expansion holds around an equilibrium point ($\dot{x} = 0$). The matrix $\tilde{\mathbf{K}}_{\mathbf{ij}}$ represents the derivatives of the vector function $f(x,u)$ with respect to $x^{(i)}$ and u^j at point (x_o,u_o). The input u is generalised to be $\alpha u(t)$, where α is any arbitrary constant. In this case, the response $x(t)$ can be expanded in terms of α as:

$$x = \sum_{i=1}^{\infty} \alpha^i x_i \quad \ldots (15)$$

By substituting in Equation (12) and rearranging according to the coefficients of equal α^i (i = 1, 2, …), a set of differential equations is generated as:

$$\begin{aligned} \dot{x}_1 &= \tilde{K}_{10}x_1 + \tilde{K}_{01}u \\ \dot{x}_2 &= \tilde{K}_{10}x_2 + \tilde{K}_{20}x_1^{(2)} + \tilde{K}_{11}x_1u + \tilde{K}_{02}u^2 \\ \dot{x}_3 &= \tilde{K}_{10}x_3 + \tilde{K}_{30}x_1^{(3)} + \tilde{K}_{20}\left[x_1 \otimes x_2 + x_2 \otimes x_1\right] + \tilde{K}_{11}x_2u + \tilde{K}_{21}x_1^{(2)}u + \tilde{K}_{12}x_1u^2 + \tilde{K}_{03}u^3 \\ &\vdots \end{aligned} \quad \ldots (16)$$

Equation (16) represents the system as an infinite set of differential equations. Although this expansion extends the n-dimensional problem to infinite dimension, the original nonlinearity of the system is broken down into a sequence of pseudo-linear time invariant (PLTI) systems, which are solvable. The input of each PLTI system is a nonlinear function of all previous system states and the input u. Figure 1 shows the schematic diagram of the method for the PLTI systems through the kth term. The first PLTI system has a linear transition matrix $\Phi(t\text{-}t_0)$ based on the square matrix $\tilde{\mathbf{K}}_{\mathbf{10}}$, which is excited by input u multiplied the column vector $\tilde{\mathbf{K}}_{\mathbf{01}}$. The state response of this system, x_1, in closed-

https://doi.org/10.1017/S0001924000007533 Published online by Cambridge University Press

form is a convolution integration in terms of u and t, which is mapped to the next system by a nonlinear function $f_i(x_1,u)$. This sequence is repeated for a certain number k, which provides satisfactory results. Note that $f_{i-1}(x_1,x_2,\ldots,x_{i-1},u)$, where $i = 1,2,\ldots,k$, automatically keeps the order of input u to the power i. For example, $f_1(x_1,u)$ is a sum of u^2, x_1u, and $x_1^{(2)}$. By substituting for x_1 as a convolution integral of u, the bilinear term, x_1u, and the state quadratic term, $x_1^{(2)}$, become a function of u_2. Then, x_2 is defined as a convolution integral of u^2. In general, this condition is not essential to the method, but it is necessary to extract the kernels. Thus, each state response of the PLTI systems, x_i, conceptually yields the kernel $h_i(\tau_1,..,\tau_i)$ as described in the next two Sections.

4.0 FIRST ORDER SYSTEM GENERALISED SOLUTION

The surge motion in Equation (7) and another roll motion presented in Refs 34-35 are examples of the SDOF first order flight system. The generalised equation of motion of such systems is

$$\begin{aligned}\dot{x} = \sum_{i=0}^{\infty}\sum_{j=0}^{\infty} k_{ij}x^i u^j = k_{10}x + k_{20}x^2 + k_{30}x^3 + \cdots + k_{01}u + k_{11}xu \\ + k_{21}x^2u + \cdots + k_{02}u^2 + k_{12}xu^2 + \cdots + k_{03}u^3 + \cdots\end{aligned} \quad \ldots (17)$$

where k_{ij} is the corresponding coefficient to the term x^iu^j and $i, j = 0,1,2,3,\ldots$ and $k_{00} = 0$. Based on the global Volterra approach in Refs 27-28, a small set of linear and nonlinear terms is enough to specify the system characteristics in a certain domain. Therefore, the quadratic state, bilinear state-input and quadratic input terms in addition to the linear terms in Equation (17) are considered sufficient. As a function of these terms, the system is

$$\dot{x} \approx ax + k_{01}u + k_{20}x^2 + k_{11}xu + k_{02}u^2 \quad \ldots (18)$$

Note the linear state term coefficient has been re-symbolised by a instead of k_{10}. This re-symbolisation has the purpose of emphasising the uniqueness of this term more than others, as clearly indicated later in this Section.

The variational method is now applied to develop the Volterra kernels. The state x can be then expressed as a

$$x = \alpha x_1 + \alpha^2 x_2 + \alpha^3 x_3 + \cdots \quad \ldots (19)$$

By substituting in Equation (18) and equating α^i coefficients, where $i = 1,2,3, \ldots$, a set of pseudo differential equations is generated as:

$$\begin{aligned}\dot{x}_1 &= ax_1 + k_{01}u \\ \dot{x}_2 &= ax_2 + k_{20}x_1^2 + k_{11}x_1u + k_{02}u^2 \\ \dot{x}_3 &= ax_3 + 2k_{20}x_1x_2 + k_{11}x_2u + k_{21}x_1^2u + k_{12}x_1u^2 \\ &\vdots\end{aligned} \quad \ldots (20)$$

The solution of the first differential equation of x_1 with a zero initial condition is

$$x_1 = k_{01}\int_0^t e^{a(t-\tau)}u(\tau)\mathrm{d}\tau \quad \ldots (21)$$

The solution of x_2 is then given as

https://doi.org/10.1017/S0001924000007533 Published online by Cambridge University Press

$$x_2 = k_{20}\int_0^t e^{a(t-\tau)}x_1^2(\tau)\mathrm{d}\tau + k_{11}\int_0^t e^{a(t-\tau)}x_1(\tau)u(\tau)\,\mathrm{d}\tau + k_{02}\int_0^t e^{a(t-\tau)}u^2(\tau)\,\mathrm{d}\tau \quad \ldots (22)$$

where x_2^{qs}, x_2^{bsi}, x_2^{qi} represent the quadratic state, bilinear state-input, and quadratic input components of x_2.

Using the convolution solution of x_1 from Equation (21) and substituting in Equation (22), the quadratic state component x_2^{qs} and the bilinear state-input component x_2^{bsi}, are then given as:

$$x_2^{qs} = \frac{k_{20}k_{01}^2}{a}\int_0^t\int_0^t e^{a(t-\tau_1)}e^{a(t-\tau_2)}\left[1-e^{a\max(t-\tau_1,t-\tau_2)}\right]u(\tau_1)u(\tau_2)\,\mathrm{d}\tau_1\mathrm{d}\tau_2 \quad \ldots (23)$$

$$x_2^{bsi} = \frac{k_{11}k_{01}}{2}\int_0^t\int_0^t\left[e^{a\max(t-\tau_1,t-\tau_2)}\right]u(\tau_1)u(\tau_2)\,\mathrm{d}\tau_1\mathrm{d}\tau_2 \quad \ldots (24)$$

where $max(x,y)$ refers to the maximum values between x and y. Note the authors documented the required mathematical manipulations to derive Equations (23-24) in Refs 34-35. The quadratic input component x_2^{qi} yields to the standard Volterra form as:

$$x_2^{qi} = k_{02}\int_0^t e^{a(t-\tau)}u^2(\tau)\,\mathrm{d}\tau = k_{02}\int_0^t\int_0^t e^{a(t-\tau_1)}\delta(\tau_1-\tau_2)u(\tau_1)u(\tau_2)\,\mathrm{d}\tau_1\mathrm{d}\tau_2 \quad \ldots (25)$$

where $\delta(\tau_1-\tau_2)$ is the impulse function.

Adding the quadratic and bilinear components to the linear term offers an approximate solution of x as

$$x \approx \int_0^t h_1(t-\tau)u(\tau)\mathrm{d}\tau + \int_0^t\int_0^t h_2(t-\tau_1,t-\tau_2)u(\tau_1)u(\tau_2)\,\mathrm{d}\tau_1\mathrm{d}\tau_2$$

where $\ldots (26)$

$$h_1(\tau) = k_{01}e^{a(\tau)}$$

$$h_2(\tau_1,\tau_2) = h_2^{qs} + h_2^{bsi} + h_2^{qi} = \frac{k_{20}k_{01}^2}{a}e^{a(\tau_1)}e^{a(\tau_2)}\left[1-e^{a\max(\tau_1,\tau_2)}\right] + \frac{k_{11}k_{01}}{2}e^{a\max(\tau_1,\tau_2)} + k_{02}e^{a(\tau_1)}\delta(\tau_1-\tau_2)$$

The resultant approximate solution is given by the two kernels h_1 and h_2. For any arbitrary input $u(t)$, one can compute the response x using convolution integrals or the pseudo state space representation. These kernels are a unique signature of the first order SDOF system. To understand how the system behaviour varies with these parameters, their influence on each kernel is presented next.

The first kernel h_1 is an exponential function with a gain k_{01} and a power factor a. It is clear that this power factor a controls the divergence or convergence of the first kernel histories. In the case of $a > 0$, the value of h_1 keeps increasing with time to be infinite as time tends to infinity. This observation concludes that the system has a divergent or unstable response for any input. If a is null, the first kernel is constant with time, which means that the system linear response is the input integration. In the case of $a < 0$, at time zero, the value of h_1 is k_{01}. This value keeps decreasing with time, yielding zero at time equal to infinity. Figure 2 shows the normalised generic shape of h_1 in the case of $a < 0$. The normalised kernel starts at 1 heading downward with an angle φ = Arctan(a). This slope is an indication of the initial or maximum speed by which the system responds to any arbitrary input. If a 2% value is considered as a tolerance for approximate steady state, the required time to be inside this zero vicinity is labeled here as the linear kernel settling time τ_{ks}^{l}. This time is computed as a function of a to be:

$$\tau_{ks}^{l} = \frac{-\ln(0\cdot02)}{|a|} \approx \frac{4}{|a|} \quad \text{for} \quad a < 0 \quad \ldots (27)$$

https://doi.org/10.1017/S0001924000007533 Published online by Cambridge University Press

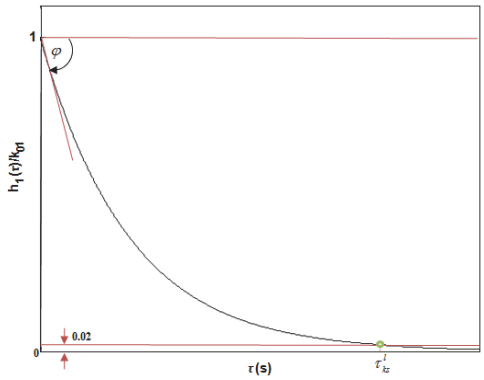


Figure 2. First order system first kernel in the case of $a < 0$.

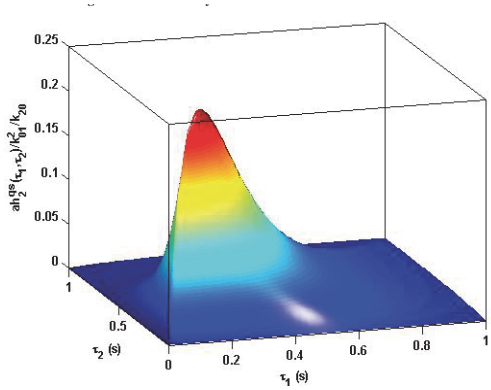


Figure 3. First order system quadratic state second kernel at $a = -5$ 1/s.

The second kernel has three components: quadratic state kernel h_2^{qs}, bilinear state-input kernel h_2^{bsi}, and quadratic input kernel h_2^{qi}. Each component is a two dimensional surface as a function of τ_1 and τ_2. The quadratic state kernel h_2^{qs} has three exponential terms. The linear coefficient a controls the divergence and convergence of this surface. In the case of $a = 0$, the expression of h_2^{qs} has undetermined value . L'Hopital's rule[36] is then applied by differentiating both the nominator and the denominator of the expression of h_2^{qs}. This gives the value $k_{20}\,x_{01}^2 max(\tau_1, \tau_2)$. This maximum operator represents two ramp surfaces τ_1 and τ_2 merged at the diagonal line, which implies that if the system is critically stable in the linear sense ($a = 0$), the state quadratic term has a divergent kernel shape (instability). Such a conclusion is not accessible using the linear analysis. When $a > 0$, the surface starts at the zero value heading upwards to a divergence referring to unstable behaviour for any external excitation. If the value of a is negative, the surface starts at zero and diminishes at infinite time arguments τ_1 and τ_2. The exponential term with the maximum operation in the exponent works on directing the surface upward and enforcing the surface edges to be zero, while the two regular exponential terms of τ_1 and τ_2 work on heading the surface downward. The irregular exponential term competes with the two regular terms reaching a maximum surface value at $\tau_1 = \tau_2 = \ln(2)/|a| \approx 0{\cdot}7/|a|$, beyond which this effect diminishes. The two standard exponential terms then dominate the shape of the surface, yielding zero as the two arguments τ_1 and τ_2 go to infinity. One example of this surface is given in Fig. 3, where $a = -5$ 1/s. The overall shape of this kernel is determined by its diagonal ($\tau_1 = \tau_2$). The normalised general shape of this diagonal is shown in Fig. 4. The surface has a maximum value $0{\cdot}25k_{20}\,k_{01}^2/a$ at time $\tau_{km}^{qs} = ln(2)/|a| \approx 0{\cdot}7/|a|$. The required time by which the surface is considered as zero is referred to here as the quadratic state kernel's settling time $\tau_{km}^{qs} = 4/|a|$.

The surface of the bilinear state-input kernel component h_2^{bsi} is an exponential function, which includes a maximum operator in the power. The surface heads to zero (stable or convergent) as τ_1 and τ_2 tend to infinity in the case of $a < 0$, or head to infinity (unstable or divergent) in the case of $a > 0$. When $a = 0$, the normalised surface is a flat one with a value 0·5.

Figure 5 shows an example of the bilinear state-input kernel at $a = -5$ 1/s. The diagonal shape of this kernel is the same as the linear first kernel in Fig. 2 with a different gain of $k_{01}k_{11}/2$, but with the same initial slope angle $\varphi = \text{Arctan}(a)$ and the same settling time $\tau_{ks}^{bsi} = \tau_{km}^{s} = 4/|a|$. The surface of the quadratic input kernel component τ_2^{qi} is an exponential impulse sheet oriented vertically on the diagonal line $\tau_1 = \tau_2$, which has the same shape and characteristics of the first kernel in Fig. 2, but with a gain of k_{02} instead of k_{01}.

https://doi.org/10.1017/S0001924000007533 Published online by Cambridge University Press

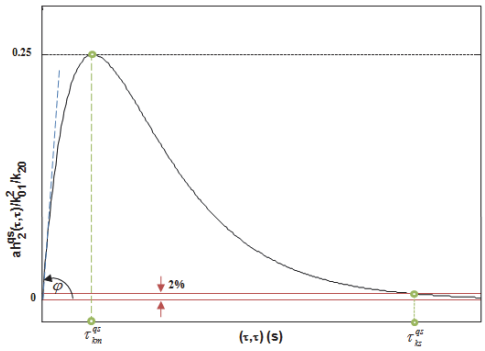


Figure 4. First order system quadratic state second diagonal kernel in the case of $a < 0$.

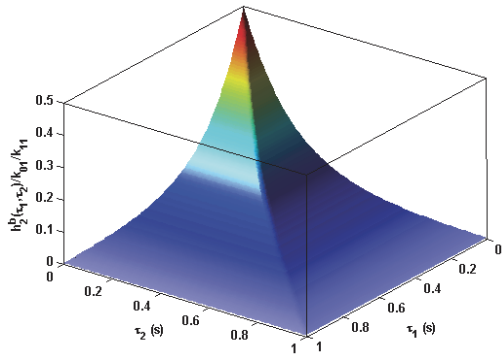


Figure 5. First order system bilinear state-input second kernel at $a = -5$ 1/s.

5.0 SECOND ORDER SYSTEM GENERALISED SOLUTION

The pitch motion in Equation (9) in addition to another yaw motion documented in Refs 34-35 are examples of the SDOF second order flight systems. The generalised equations of motion of such systems are:

$$\begin{aligned}\dot{x} &= v \\ \dot{v} &= -\omega_n^2 x - 2\zeta\omega_n v + k_{200}x^2 + k_{110}xv + k_{020}v^2 \quad + k_{001}u \; + k_{101}xu + k_{011}vu + k_{002}u^2\end{aligned} \qquad \ldots (28)$$

Parameter k_{lmn} is the corresponding coefficient to the term $x^l v^m u^n$ and l, m, n = 0,1,2. Note that the linear terms have been re-symbolised by $-2\zeta\omega_n$ instead of k_{010} and $-\omega_n^2$ instead of k_{100}. This re-symbolisation is for the purpose of keeping the discussion in the sense of undamped natural frequency ωn and damping ratio ζ from the linear theory. The variational method is now applied to Equation (28) to develop the kernels. The method assumes that the input is αu where α is any arbitrary constant. The state position x and state rate v can then be expressed as a sum of infinite terms.

$$\begin{aligned}x &= \alpha x_1 + \alpha^2 x_2 + \alpha^3 x_3 + \cdots \\ v &= \alpha v_1 + \alpha^2 v_2 + \alpha^3 v_3 + \cdots\end{aligned} \qquad \ldots (29)$$

By equating α^i coefficient, a set of pseudo differential equations is generated:

$$\begin{aligned}
&\begin{bmatrix}\dot{x}_1 \\ \dot{v}_1\end{bmatrix} = \begin{bmatrix}0 & 1 \\ -\omega_n^2 & -2\zeta\omega_n\end{bmatrix}\begin{bmatrix}x_1 \\ v_1\end{bmatrix} + \begin{bmatrix}0 \\ k_{001}\end{bmatrix}u \\
&\begin{bmatrix}\dot{x}_2 \\ \dot{v}_2\end{bmatrix} = \begin{bmatrix}0 & 1 \\ -\omega_n^2 & -2\zeta\omega_n\end{bmatrix}\begin{bmatrix}x_2 \\ v_2\end{bmatrix} + \begin{bmatrix}0 \\ k_{200}x_1^2\end{bmatrix} + \begin{bmatrix}0 \\ k_{110}x_1v_1\end{bmatrix} + \begin{bmatrix}0 \\ k_{020}v_1^2\end{bmatrix} + \begin{bmatrix}0 \\ k_{101}x_1u\end{bmatrix} + \begin{bmatrix}0 \\ k_{011}v_1u\end{bmatrix} + \begin{bmatrix}0 \\ k_{002}u^2\end{bmatrix} \\
&\begin{bmatrix}\dot{x}_3 \\ \dot{v}_3\end{bmatrix} = \begin{bmatrix}0 & 1 \\ -\omega_n^2 & -2\zeta\omega_n\end{bmatrix}\begin{bmatrix}x_3 \\ v_3\end{bmatrix} + \cdots \\
&\vdots
\end{aligned} \qquad \ldots (30)$$

https://doi.org/10.1017/S0001924000007533 Published online by Cambridge University Press

The solution of the first linear pseudo subsystem $[x_1\ v_1]^T$ for a zero initial condition is then computed as

$$x_1 = \frac{k_{001}}{\omega_d}\int_0^t e^{-\sigma(t-\tau)}\mathrm{Sin}\left(\omega_d(t-\tau)\right)u(\tau)\,\mathrm{d}\tau$$
$$v_1 = \frac{-k_{001}}{\sqrt{1-\zeta^2}}\int_0^t e^{-\sigma(t-\tau)}\mathrm{Sin}\left(\omega_d(t-\tau)-\varphi\right)u(\tau)\,\mathrm{d}\tau\,,\quad \varphi = \mathrm{Cos}^{-1}(\zeta) \qquad \ldots (31)$$

where $\sigma = \zeta\omega_n$ denotes the system's damping factor and $\omega_d = \omega_n\sqrt{1-\zeta^2}$ is the damped natural frequency.

For the second pseudo subsystem $[x_2\ v_2]^T$, the solution of x_2 is sought as a sum of six components

$$x_2 = x_2^{qs} + x_2^{bsr} + x_2^{qr} + x_2^{bsi} + x_2^{bri} + x_2^{qi} \qquad \ldots (32)$$

where x_2^{qs}, x_2^{bsr}, x_2^{qr}, x_2^{bsi}, x_2^{bri} and x_2^{qi} are quadratic state, bilinear state-rate, quadratic rate, bilinear state-input, bilinear rate-input, and quadratic input component respectively. The second pseudo state space is then rewritten as:

$$\begin{bmatrix}\dot{x}_2\\ \dot{v}_2\end{bmatrix} = \underbrace{\begin{bmatrix}0 & 1\\ -\omega_n^2 & -2\zeta\omega_n\end{bmatrix}}_{A}\begin{bmatrix}x_2\\ v_2\end{bmatrix} + \underbrace{\begin{bmatrix}0\\ k_{200}\end{bmatrix}}_{B_{qs}}x_1^2 + \underbrace{\begin{bmatrix}0\\ k_{110}\end{bmatrix}}_{B_{bsr}}x_1v_1 + \underbrace{\begin{bmatrix}0\\ k_{020}\end{bmatrix}}_{B_{qr}}v_1^2 + \underbrace{\begin{bmatrix}0\\ k_{101}\end{bmatrix}}_{B_{bsi}}x_1u + \underbrace{\begin{bmatrix}0\\ k_{011}\end{bmatrix}}_{B_{bri}}v_1u \qquad \ldots (33)$$

Substituting the convolution solutions of x_1 and v_1 from Equation (31) into Equation (33), the convolution solutions of the six components of x_2 are derived as[34-35]:

$$x_2^{qs} = \int_0^t\int_0^t h_2^{qs}(t-\tau_1,t-\tau_2)u(\tau_1)u(\tau_2)\,\mathrm{d}\tau_1\mathrm{d}\tau_2$$
$$h_2^{qs}(\tau_1,\tau_2) = \frac{k_{200}k_{001}^2}{2\omega_d^4}e^{-\sigma\tau_1}e^{-\sigma\tau_2}\left\{M_1\mathrm{Cos}\left(\omega_d(\tau_1-\tau_2)\right)+M_2\mathrm{Cos}\left(\omega_d(\tau_1+\tau_2)\right)+M_3\mathrm{Sin}\left(\omega_d(\tau_1+\tau_2)\right)\right\} \qquad \ldots (34)$$

$$x_2^{bsr} = \int_0^t\int_0^t h_2^{bsr}(t-\tau_1,t-\tau_2)u(\tau_1)u(\tau_2)\,\mathrm{d}\tau_1\mathrm{d}\tau_2$$
$$h_2^{bsr}(\tau_1,\tau_2) = \frac{k_{110}k_{001}^2}{2\sqrt{1-\zeta^2}\omega_d^3}e^{-\sigma\tau_1}e^{-\sigma\tau_2}\left\{M_1\mathrm{Cos}\left(\omega_d(\tau_1-\tau_2)+\varphi\right)\right.$$
$$\left.+M_2\mathrm{Cos}\left(\omega_d(\tau_1+\tau_2)-\varphi\right)\ +M_3\mathrm{Sin}\left(\omega_d(\tau_1+\tau_2)-\varphi\right)\right\} \qquad \ldots (35)$$

$$x_2^{qr} = \int_0^t\int_0^t h_2^{qr}(t-\tau_1,t-\tau_2)u(\tau_1)u(\tau_2)\,\mathrm{d}\tau_1\mathrm{d}\tau_2$$
$$h_2^{qr}(\tau_1,\tau_2) = \frac{k_{020}k_{001}^2}{2\left(1-\zeta^2\right)\omega_d^2}e^{-\sigma\tau_1}e^{-\sigma\tau_2}\left\{\begin{matrix}M_1\mathrm{Cos}\left(\omega_d(\tau_1-\tau_2)\right)\\ +M_2\mathrm{Cos}\left(\omega_d(\tau_1+\tau_2)-2\varphi\right)\end{matrix}+M_3\mathrm{Sin}\left(\omega_d(\tau_1+\tau_2)-2\varphi\right)\right\} \qquad \ldots (36)$$

$$x_2^{bsi} = \int_0^t\int_0^t h_2^{bsi}(t-\tau_1,t-\tau_2)u(\tau_1)u(\tau_2)\,\mathrm{d}\tau_1\mathrm{d}\tau_2$$
$$h_2^{bsi}(\tau_1,\tau_2) = \frac{k_{001}k_{101}}{2\omega_d^2}e^{-\sigma\max(\tau_1,\tau_2)}\left\{\mathrm{Sin}\left(\omega_d\min(\tau_1,\tau_2)\right)\mathrm{Sin}\left(\omega_d\max(\tau_1,\tau_2)-\omega_d\min(\tau_1,\tau_2)\right)\right\} \qquad \ldots (37)$$

https://doi.org/10.1017/S0001924000007533 Published online by Cambridge University Press

$$x_2^{bri} = \int_0^t \int_0^t h_2^{bri}(t-\tau_1, t-\tau_2)\, u(\tau_1)\, u(\tau_2)\, d\tau_1 d\tau_2$$
$$h_2^{bri}(\tau_1,\tau_2) = \frac{-k_{011}k_{001}}{2\omega_d\sqrt{1-\zeta^2}} e^{-\sigma\max(\tau_1,\tau_2)} \left\{ \mathrm{Sin}\left(\omega_d \min(\tau_1,\tau_2)\right) \mathrm{Sin}\left(\omega_d \max(\tau_1,\tau_2) - \omega_d \min(\tau_1,\tau_2) - \varphi\right) \right\} \quad \ldots (38)$$

$$x_2^{qi} = \int_0^t \int_0^t h_2^{qi}(t-\tau_1, t-\tau_2)\, u(\tau_1)\, u(\tau_2)\, d\tau_1 d\tau_2$$
$$h_2^{qi}(\tau_1,\tau_2) = \frac{k_{002} e^{-\sigma(\tau_1)}}{\omega_d} \mathrm{Sin}\left(\omega_d(\tau_1)\right) \delta(\tau_1 - \tau_2) \quad \ldots (39)$$

where

$$M_1(\tau_1,\tau_2) = \left(1-\zeta^2\right)\left\{1 + \frac{e^{\sigma\min(\tau_1,\tau_2)}}{\sqrt{1-\zeta^2}} \mathrm{Sin}\left(\omega_d \min(\tau_1,\tau_2) - \varphi\right)\right\}$$

$$M_2(\tau_1,\tau_2) = \frac{\left(1-\zeta^2\right)}{2}\left\{1 + \frac{e^{\sigma\min(\tau_1,\tau_2)}}{\sqrt{1-\zeta^2}} \mathrm{Sin}\left(\omega_d \min(\tau_1,\tau_2) - \varphi\right)\right\}$$
$$- \frac{3\left(1-\zeta^2\right)}{2\left(9-8\zeta^2\right)}\left\{1 + \sqrt{\frac{9-8\zeta^2}{9-9\zeta^2}} e^{\sigma\min(\tau_1,\tau_2)} \mathrm{Sin}\left(3\omega_d \min(\tau_1,\tau_2) - \hat{\varphi}\right)\right\}$$

$$M_3(\tau_1,\tau_2) = \frac{\zeta\sqrt{1-\zeta^2}}{2}\left\{1 - \frac{e^{\sigma\min(\tau_1,\tau_2)}}{\zeta} \mathrm{Cos}\left(\omega_d \min(\tau_1,\tau_2) - \varphi\right)\right\}$$
$$- \frac{\zeta\sqrt{1-\zeta^2}}{2\left(9-8\zeta^2\right)}\left\{1 - \frac{\sqrt{9-8\zeta^2}}{\zeta} e^{\sigma\min(\tau_1,\tau_2)} \mathrm{Cos}\left(3\omega_d \min(\tau_1,\tau_2) - \hat{\varphi}\right)\right\}$$

and $\mathrm{Cos}(\hat{\varphi}) = \zeta/\sqrt{9-8\zeta^2}$. The authors provided a full derivation to the expressions of Equations (34)-(39) in Refs 34-35. The overall second kernel is a sum of the six components quadratic state h_2^{qs}, bilinear state-rate h_2^{bsr}, quadratic rate h_2^{qr}, bilinear state-input h_2^{bsi}, bilinear rate-input h_2^{bri}, and quadratic input h_2^{qi}.

The resultant second kernel along with the first kernel represents an approximate Volterra-based model for the second order SDOF system.

$$x \approx \int_0^t h_1(t-\tau)\, u(\tau) d\tau + \int_0^t \int_0^t h_2(t-\tau_1, t-\tau_2)\, u(\tau_1)\, u(\tau_2)\, d\tau_1 d\tau_2$$
$$h_2 = h_2^{qs} + h_2^{bsr} + h_2^{qr} + h_2^{bsi} + h_2^{bri} + h_2^{qi} \quad \ldots (40)$$

The Volterra-based model presents the system as two analytical kernels. The analytical expressions of these kernels are used to understand each kernel characteristic as a function of system parameters for the second order SDOF system.

The first kernel h_1 is an exponential sinusoidal function with a gain k_{001}/ω_d , frequency ω_d and a damping factor σ. If the damping factor is less than zero, then the system lacks the damping required to stabilise the response for any excitation. Thus, the positive exponential power shapes a divergent kernel. When taking the damping factor off (null damping factor), the remaining sine term keeps the kernel shape as an oscillatory one. In the case of positive damping factor $\sigma > 0$, it

https://doi.org/10.1017/S0001924000007533 Published online by Cambridge University Press

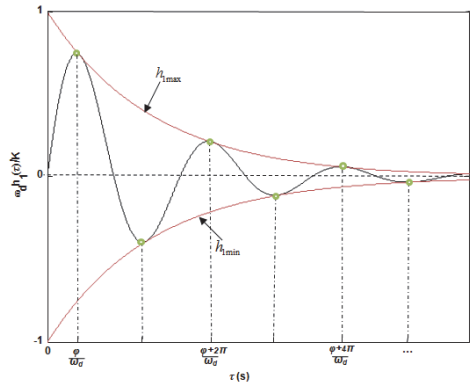


Figure 6. Second order system first kernel in the case of $0 < \zeta < 1$.

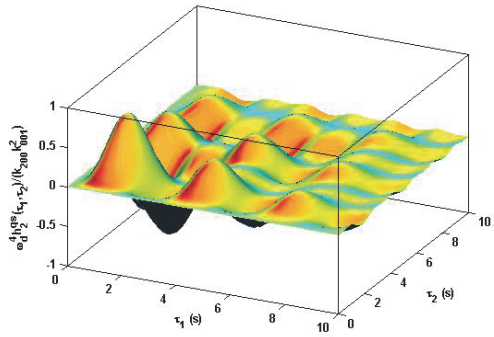


Figure 7. Second order system quadratic state kernel at ζ = 0·1 and ω_n = 2 rad/s.

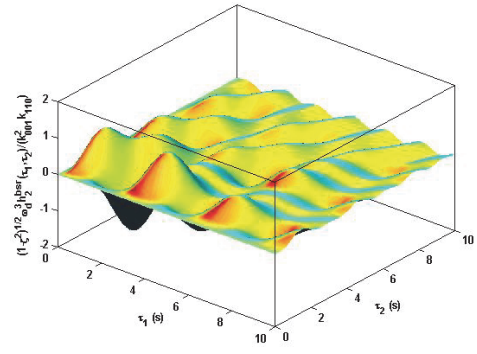


Figure 8. Second order system bilinear state-rate kernel at ζ = 0·1 and ω_n = 2 rad/s.

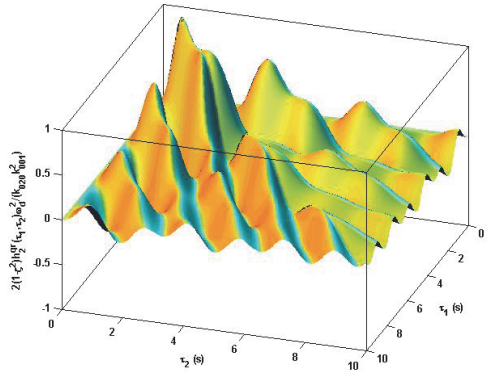


Figure 9. Second order system quadratic rate kernel at ζ = 0·1 and ω_n = 2 rad/s.

is better to parameterise the kernel by the damping ratio $\zeta = \sigma/\omega_n$. If the damping ratio is more than or equal to unity, then the sine term diminishes and the resultant first kernel is a sum of two exponential terms, which is the case in the first order system. These two exponential terms become equal at $\zeta = 1$. For less than unity damping ratio $0 < \zeta < 1$, the generic shape of the first kernel is shown in Fig. 6. In this case ($0 < \zeta < 1$), the kernel starts at zero and oscillates around zero. The amplitude of such oscillation decreases with time, where the loci of minimum and maximum points are located along the envelope functions h_{1max} and h_{1min}.

$$h_{1max}(t) = \frac{k_{001}}{\omega_d} e^{-\sigma t}, \quad h_{1min}(t) = -\frac{k_{001}}{\omega_d} e^{-\sigma t} \qquad \ldots (41)$$

The maximum points occur at times $(2n\pi+\varphi)/\omega_d$, while the minimum points occur at times $((2n+1)\pi+\varphi)/\omega_d$, where $n = 0,1,2,\ldots$ The kernel h_1 settles down inside a 2% band around zero at time

$$\tau_{ks}^{l} = \frac{-\ln(0{\cdot}02)}{\sigma} \approx \frac{4}{\sigma} \quad \text{for } 0 < \varsigma < 1 \qquad \ldots (42)$$

https://doi.org/10.1017/S0001924000007533 Published online by Cambridge University Press

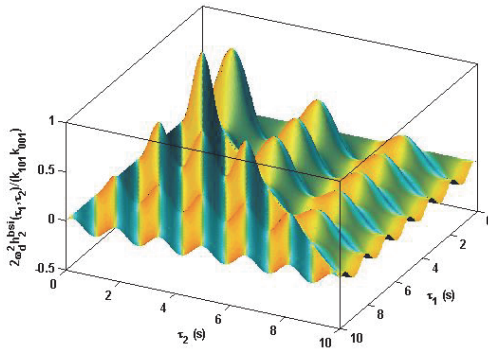


Figure 10. Second order system bilinear state-input kernel at ζ= 0·1 and ω_n = 2 rad/s.

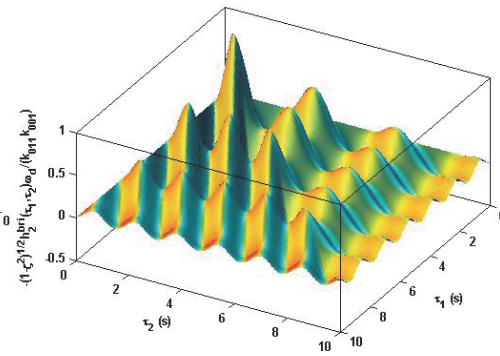


Figure 11. Second order system bilinear rate-input kernel at ζ = 0·1 and ω_n = 2 rad/s.

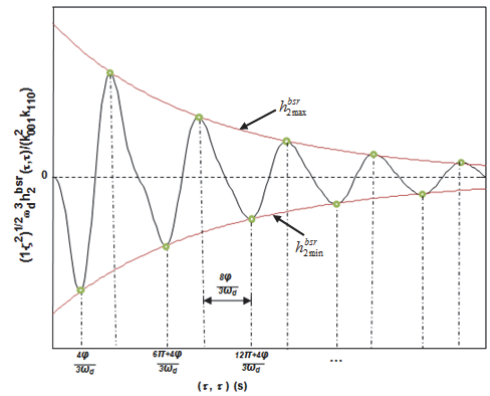


Figure 12. Second order system quadratic state diagonal kernel in the case of 0 < ζ < 1.

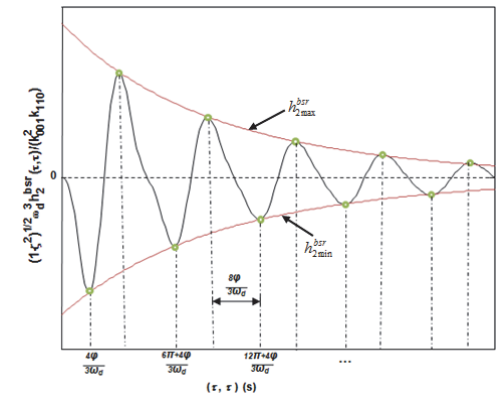


Figure 13. Second order system bilinear state-rate diagonal kernel in the case of 0 < ζ < 1.

The second kernel has six components: h_2^{qs}, h_2^{bsr}, h_2^{qr}, h_2^{bsi}, h_2^{bri} and h_2^{qi}. Each component is a two dimensional surface in τ_1 and τ_2. In the case of negative damping factor σ, all the surfaces have zero edges heading upwards to infinity as τ_1 and τ_2 go to infinity. These divergent surfaces have a sinusoidal waveform with a frequency ω_d in the case of $-1 < \zeta < 0$ (oscillatory divergent). This sinusoidal waveform diminishes when ζ –1 (non-oscillatory divergent). All surfaces become a constant amplitude two-dimensional sinusoidal surface in the case of zero damping ratio $\zeta = 0$ (oscillatory). No parametric studies are given to the unstable or critically stable cases, since these cases have a divergent response, which does not require to be characterised. Thus, the characterisation is sought for a stable behaviour for the design and control purposes. If the damping ratio is more than unity $\zeta \geq 1$ (non-oscillatory convergent), all the surfaces turn to a sum of two exponential functions and the analysis of the first order system in Section IV can then be used. In the case of $0 < \zeta < 1$ (oscillatory convergent), which is the frequent case of the aircraft low order motions, all the surfaces have a two-dimensional damped sinusoidal waveform. One example is given in Figs 7-11 at $\zeta = 0{\cdot}1$ and $\omega_n = 2$ rad/s. The quadratic input component, as a special case, is an impulsive surface over the diagonal line $\tau_1 = \tau_2$ having the same shape as the first kernel but with a gain of k_{002}/ω_d.

In order to characterise each surface in the case of $0 < \zeta < 1$, the diagonal waveform $h_2^j(\tau,\tau)$ where $j = \{qs, bsr, qr, bri\}$, is considered, while the diagonal waveform of $h_2^{bsi}(\tau, 0\,5\tau)$ is considered. Thus,

https://doi.org/10.1017/S0001924000007533 Published online by Cambridge University Press

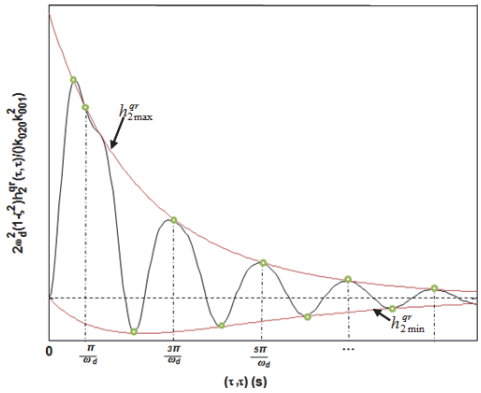


Figure 14. Second order system quadratic rate diagonal kernel in the case of $0 < \zeta < 1$.

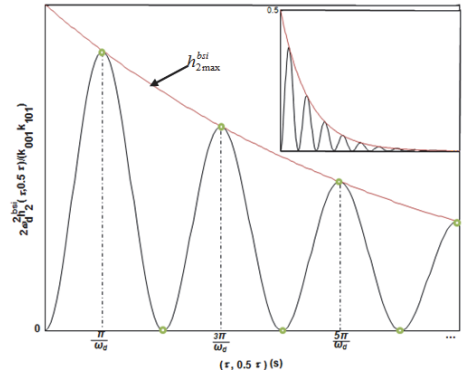


Figure 15. Second order system bilinear state-input diagonal kernel in the case of $0 < \zeta < 1$.

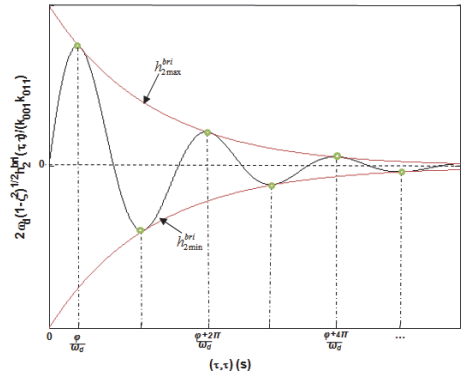


Figure 16. Second order system bilinear rate-input diagonal kernel in the case of $0 < \zeta < 1$.

Table 1
The times of maximum and minimum values of the second kernel's components, where $n = 0, 1, 2, \ldots$

Nonlinear component	Time of minimum values (s)	Time of maximum values (s)
Quadratic state component $h_2^{qs}(\tau,\tau)$	$(2n\pi)/\omega_d$	$((2n+1)\pi)/\omega_d$
Bilinear state-rate component $h_2^{bsr}(\tau,\tau)$	$(6n\pi+4\varphi)/3/\omega_d$	$(6n\pi-4\varphi)/3/\omega_d$
Quadratic rate component $h_2^{qr}(\tau,\tau)$	$(2n\pi)/\omega_d$	$((2n+1)\pi)/\omega_d$
Bilinear state-input component $h_2^{bsi}(\tau,0\ 5\tau)$	$(2n\pi)/\omega_d$	$((2n+1)\pi)/\omega_d$
Bilinear rate-input component $h_2^{bri}(\tau,\tau)$	$(2n\pi+\varphi)/\omega_d$	$((2n+1)\pi+\varphi)/\omega_d$

the diagonal line of $h_2^{bsi}(\tau,\tau)$ has a zero waveform. Figures 12-16 show the generic shapes of these diagonal waveforms. All the diagonal histories start at zero value and oscillate by a frequency ω_d generating a set of minimum and maximum value at times listed in Table 1.

Although all the diagonal waveforms settle at zero by time $t = \infty$, the equivalent oscillation shapes to reach this zero value are not the same. Both quadratic state $h_2^{qs}(\tau,\tau)$ in Fig. 12 and quadratic rate $h_2^{qr}(\tau,\tau)$ in Fig. 14 do not symmetrically oscillate around the zero value. The mean oscillation shapes of $h_2^{qs}(\tau,\tau)$ and $h_2^{qr}(\tau,\tau)$ are similar to the one in Fig. 4 (the quadratic state diagonal kernel of the

https://doi.org/10.1017/S0001924000007533 Published online by Cambridge University Press

first order system). The mean oscillation shape is sought here as the average of the maximum and minimum points' loci. If the average of these loci is constant, as in the case of first kernel, the oscillation shape is then symmetrical. The two components $h_2^{qs}(\tau,\tau)$ and $h_2^{qr}(\tau,\tau)$ have the same mathematical structure as listed in Equation (34) and Equation (36), except the phase shift $-\varphi$ in the two arguments. This phase shift warps the diagonal lines of $h_2^{qr}(\tau,\tau)$ from the diagonal lines of $h_2^{qs}(\tau,\tau)$ (as an example, see Figs 7 and 9). Because of this phase shift, there is one non-periodic maximum point in the case of $h_2^{qr}(\tau,\tau)$, which appears at time $4\varphi/3\pi$ (see Fig. 14). On the other hand, the diagonal waveform of the bilinear state-input component $h_2^{bsi}(\tau,0\,5\tau)$ in Fig. 15 has a mean oscillation shape similar to the bilinear state-input diagonal waveform in Fig. 5. Both the diagonal forms of the bilinear state-rate h_2^{bsi} in Fig. 13 and bilinear rate-input h_2^{bri} in Fig. 16 symmetrically oscillate around zero.

The loci of the maximum and minimum points are developed by substituting their equivalent times in Equations (34-38), which leads to:

$$h_{2\min}^{qs}=\frac{k_{200}k_{001}^2}{\omega_d^4}\psi_1(\zeta)\left(e^{-2\sigma t}-e^{-\sigma t}\right),\quad h_{2\max}^{qs}=\frac{k_{200}k_{001}^2}{\omega_d^4}\psi_1(\zeta)\left(e^{-2\sigma t}+e^{-\sigma t}\right)$$
$$\psi_1(\zeta)=\frac{2\left(1-\zeta^2\right)\left(3-2\zeta^2\right)}{\left(9-8\zeta^2\right)} \qquad \ldots (43)$$

$$h_{2\max}^{bsr}=\frac{-k_{110}k_{001}^2}{2\sqrt{1-\zeta^2}\,\omega_d^3}\left\{\psi_2(\zeta)e^{-2\sigma t}+\psi_3(\zeta)e^{-\sigma t}\right\},\quad h_{2\min}^{bsr}=\frac{-k_{110}k_{001}^2}{2\sqrt{1-\zeta^2}\,\omega_d^3}\left\{\psi_4(\zeta)e^{-2\sigma t}+\psi_5(\zeta)e^{-\sigma t}\right\}$$

$$\psi_2(\xi)=\zeta\left(1-\zeta^2\right)+\frac{\left(1-\zeta^2\right)\left(3-4\zeta^2\right)}{\left(9-8\zeta^2\right)}\mathrm{Cos}\left(\frac{5\varphi}{3}\right)+\frac{4\zeta\left(1-\zeta^2\right)^{3/2}}{\left(9-8\zeta^2\right)}\mathrm{Sin}\left(\frac{5\varphi}{3}\right)$$
$$\psi_3(\xi)=\sqrt{1-\zeta^2}\left\{\zeta\mathrm{Sin}\left(\frac{\varphi}{3}\right)-\frac{1}{2}\mathrm{Sin}\left(\frac{7\varphi}{3}-\hat{\varphi}\right)\right\}-\frac{1}{2}\sqrt{\frac{1-\zeta^2}{9-8\zeta^2}}\mathrm{Sin}\left(\frac{4\varphi}{3}\right) \qquad \ldots (44)$$
$$\psi_4(\xi)=\frac{\left(1-\zeta^2\right)}{\left(9-8\zeta^2\right)}\left\{\zeta\left(9-8\zeta^2\right)+\left(3-4\zeta^2\right)\mathrm{Cos}(11\varphi/3)-4\zeta\sqrt{1-\zeta^2}\mathrm{Sin}(11\varphi/3)\right\}$$
$$\psi_5(\xi)=\frac{\sqrt{1-\zeta^2}}{2}\left\{\mathrm{Sin}(4\varphi/3)-2\zeta\mathrm{Sin}(7\varphi/3)+\frac{1}{\sqrt{9-8\zeta^2}}\mathrm{Sin}(\varphi/3+\hat{\varphi})\right\}$$

$$h_{2\min}^{qr}=\frac{k_{020}k_{001}^2}{2\left(1-\zeta^2\right)\omega_d^2}\psi_6(\zeta)\left(e^{-2\sigma t}-e^{-\sigma t}\right),\quad h_{2\max}^{qr}=\frac{k_{020}k_{001}^2}{2\left(1-\zeta^2\right)\omega_d^2}\psi_6(\zeta)\left(e^{-2\sigma t}+e^{-\sigma t}\right)$$
$$\psi_6(\varsigma)=1-\zeta^2+\frac{\left(1-\zeta^2\right)\left(4-3\zeta^2\right)}{\left(9-8\zeta^2\right)}\left\{\mathrm{Cos}(2\varphi)+\frac{4\zeta\sqrt{1-\zeta^2}}{\left(4-3\zeta^2\right)}\mathrm{Sin}(2\varphi)\right\} \qquad \ldots (45)$$

$$h_{2\max}^{bsi}(\tau,0\cdot5\tau)=\frac{k_{101}k_{001}}{2\omega_d^2}e^{-\sigma t},\quad h_{2\min}^{bsi}(\tau,0\cdot5\tau)=0 \qquad \ldots (46)$$

https://doi.org/10.1017/S0001924000007533 Published online by Cambridge University Press

Table 2
The settling time of the diagonal second kernel's components

Nonlinear component	Settling time (s)
Quadratic state component $h_2^{qs}(\tau,\tau)$	$\tau_{ks}^{qs} = \frac{1}{\sigma}\ln\left\{\frac{2}{-1+\sqrt{1+0\cdot08/\psi_1(\varsigma)}}\right\}$
Bilinear state-rate component $h_2^{bsr}(\tau,\tau)$	$\tau_{ks}^{bsr} = \frac{1}{\sigma}\ln\left\{\frac{2\psi_4(\zeta)}{-\psi_5(\zeta)+\sqrt{\psi_5^2(\zeta)+0\cdot08\psi_4(\zeta)}}\right\}$
Quadratic rate component $h_2^{qr}(\tau,\tau)$	$\tau_{ks}^{qr} = \frac{1}{\sigma}\ln\left\{\frac{2}{-1+\sqrt{1+0\cdot08/\psi_6(\varsigma)}}\right\}$
Bilinear state-input component $h_2^{bsi}(\tau,0\ 5\tau)$	$\tau_{ks}^{bsi} = \frac{4}{\sigma}$
Bilinear rate-input component $h_2^{bri}(\tau,\tau)$	$\tau_{ks}^{bri} = \frac{-\ln\left(0\cdot02/\left(1-\zeta^2\right)\right)}{\sigma}$

$$h_{2\max}^{bri}(\tau,\tau) = \frac{k_{011}k_{001}}{2\omega_d\sqrt{1-\zeta^2}}e^{-\sigma t}\ ,\ h_{2\min}^{bri}(\tau,\tau) = \frac{-k_{011}k_{001}}{2\omega_d\sqrt{1-\omega^2}}e^{-\sigma t} \qquad \ldots (47)$$

where h_{2min}^{j} and h_{2max}^{j} are the loci of minimum and maximum values of the diagonal signals, where $j = \{qs, bsr, qr, bsi, bri\}$. The amplitude of these maximum and minimum loci yields to a zero value at time τ tends to infinity. If a 2% vicinity is considered as a tolerance to approximate steady state of each second kernel's component, the required time to be inside the vicinity of each component is given in Table 2. These 2% vicinities are considered from the normalised gain of each component. The settling times in Table 2 are estimators to the settling times of the total surface of each component.

The developed analytical kernels in Sections IV and V predict the behaviour of the system for any arbitrary input. For the first term in the solution x_1, the single convolution integral sums up the contributions from past inputs weighted by the first kernel's behaviour across this past time span. Both first kernel of the first order system in Fig. 2 and of the second order system in Fig. 6 show that more recent inputs are more heavily counted than inputs in the distant past. The second term in the solution x_2 is determined in a similar way across a double convolution integral involving: the three components in the case of the first order system and six components in the case of the second order system. Each nonlinear component simultaneously counts the input signal at two different times τ_1 and τ_2. The next two Sections focus on the step response as a more specific case in qualifying the nonlinear dynamic behaviour.

6.0 FIRST ORDER SYSTEM STEP RESPONSE

The response to a step input is selected herein as the baseline to characterise the system behaviour of the first order SDOF. Using Equation (26) to compute the step response of each component individually, the system overall step response is then sought as:

https://doi.org/10.1017/S0001924000007533 Published online by Cambridge University Press

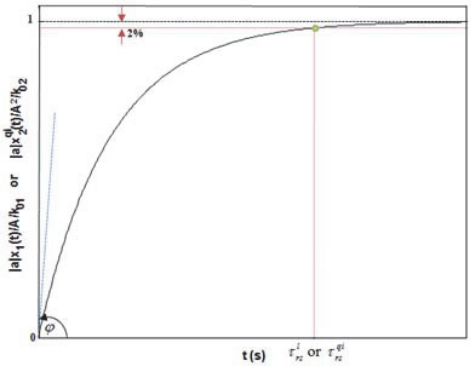


Figure 17. First order system linear or quadratic input response to step input ($a < 0$).

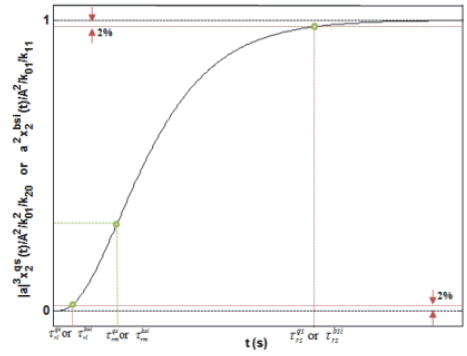


Figure 18. First order system quadratic state or bilinear state-input response to step input ($a < 0$).

$$x \approx x_1 + \underbrace{x_2^{qs} + x_2^{bsi} + x_2^{qi}}_{x_2}$$

$$x_1 = \frac{Ak_{01}}{a}\left(e^{at}-1\right), \quad x_2^{qi} = \frac{A^2k_{02}}{a}\left(e^{at}-1\right) \qquad \ldots (48)$$

$$x_2^{qs} = \frac{A^2k_{01}^2k_{20}}{a^3}\left(e^{2at}-2ate^{at}-1\right), \quad x_2^{bsi} = \frac{A^2k_{01}k_{11}}{a^2}\left(1-e^{at}+ate^{at}\right)$$

In Equation (48), A is the step input amplitude. The four terms x_1, $x_2{}^{qs}$, $x_2{}^{bsi}$ and $x_2{}^{qi}$ are the contributions of the linear, quadratic, and bilinear components in the system behaviour. Assembling these components together presents the overall response. To show each component's effect on the overall behaviour, the generic shape of each term is individually visualised as shown in Figs 17 and 18 in the case of $a < 0$. Both linear and quadratic input components have the same mathematical structure except for the steady gain as shown in Fig. 17. Although the normalised state quadratic and bilinear components have different mathematical structure, both yield the same generic shape as shown in Fig. 18 but with different parameters.

All responses start at zero and head upward. The initial slope of the normalised linear and input bilinear terms is Tan(φ) = a, while both the normalised state quadratic and bilinear terms have a zero initial slope. This observation indicates that both state quadratic and bilinear terms have no influence on the initial rate in which the system behaves for any input excitation. The initial rate $\dot{x}(0)$ is a function of the ratio between the linear coefficient k_{01} and the quadratic input coefficient k_{02} in addition to the input amplitude A. For example, if input quadratic coefficient k_{02} has a negative sign and the coefficient k_{01} has a positive sign, the total initial rate is then less than the expected one from the linear analysis and there may be an undershoot phenomena that appears in the case when the input quadratic coefficient k_{02} is more dominant or at a high input amplitude A.

Both the state quadratic and bilinear responses have a noticeable lag. The duration of lag in the state quadratic term is longer than in the case of the bilinear term but its transient rise is steeper. Thus, the quadratic kernel has zero edges and the bilinear kernel has non-zero edges. Referring to these two lags as τ_{r1}^{qs} and τ_{r1}^{bsi}, if 2% is considered as the required threshold to leave the vicinity of such a lag, then these two lags are approximately found to be 0·45/|a| and 0·2/|a|. Note that the quadratic and bilinear step responses include a ramp function multiplied by an exponential function, which sets hurdles in computing their lag times analytically; a reason for which numerical fitting is considered. These time lags are the instances at which a deviation between linear

https://doi.org/10.1017/S0001924000007533 Published online by Cambridge University Press

and nonlinear simulation starts to be significant in the case of a zero input quadratic coefficient, which is frequently observed in aircraft applications.

The deviation between linear and nonlinear responses can be positive or negative depending on the difference in signs between the linear coefficient and both the x_2^{qs} and x_2^{bsi} coefficients. This deviation widens due to an increase in the slopes of the state quadratic and bilinear terms, after the two terms exit from their lag vicinity. This increasing slope reaches a maximum at time $\tau_{rm}^{qs} = 1{\cdot}6/|a|$ and $\tau_{rm}^{bsi} = 1/|a|$ for x_2^{qs} and x_2^{b} respectively, which are computed using numerical fitting. After reaching these maximum slopes, a rapid decrease in each term's rate leads to an offset difference between the linear and nonlinear responses. Sequentially, each term settles to its steady gain at equivalent settling times $\tau_{rs}^{1} = \tau_{rs}^{qi} = 4/|a|$ in the case of the linear and input quadratic terms, $\tau_{rs}^{qs} = 6{\cdot}6/|a|$ in the case of the state quadratic term, and $\tau_{rs}^{bsi} = 5{\cdot}8/|a|$ in the case of the bilinear term. The overall response settles at:

$$x_{ss} = \frac{Ak_{01}}{|a|} + \frac{A^2k_{01}^2k_{20}}{|a|a^2} + \frac{A^2k_{01}k_{11}}{a^2} + \frac{A^2k_{02}}{|a|} \quad \ldots (49)$$

The time for reaching this steady value depends on the ratio between the coefficients of each term and the input amplitude. For example, if the system has only a state quadratic nonlinearity and this term has a negative sign, which means negative x_2^{qs}, the settling time in this case is less than the linear settling time, since the system settles before the steady value of the linear term. Such observation reveals that nonlinearity may sometimes improve the system behaviour.

The resultant analytical Volterra-based model for the first order SDOF system illuminates many of the nonlinearities usually observed in experimental and numerical results such as the amplitude-dependency response, or how the system becomes non-homogenous with increasing input amplitude. Hence, changing the amplitude not only changes the steady value of the output but also changes the shape through which the system reaches this steady value. Also, the linear coefficient a not only controls the stability of the system but also controls the system nonlinearity strength. For example, in the case of a highly damped system, if the system is weakly nonlinear or the nonlinear terms are neglected compared to the linear terms, the system then behaves close to a linear one. On the other hand, if the system lacks sufficient damping, the nonlinearity cannot be neglected even though the nonlinear terms are small. Thus, the low stability gain a increases the significance of the second order quadratic state kernel and instability possibly arises before the condition $a = 0$.

7.0 SECOND ORDER SYSTEM STEP RESPONSE

Recall Equation (40) and assume a step input with amplitude A excites the system, the approximate step response of this nonlinear system is then:

$$x = x_1 + \underbrace{x_2^{qp} + x_2^{bpr} + x_2^{qr} + x_2^{bpi} + x_2^{bri} + x_2^{qi}}_{x_2} \quad \ldots (50)$$

where

$$x_1 = \frac{k_{001}A}{\omega_n^2}\left\{1 - \frac{e^{-\sigma t}}{\sqrt{1-\zeta^2}}\mathrm{Sin}\left(\omega_d t + \varphi\right)\right\} \quad \ldots (51)$$

https://doi.org/10.1017/S0001924000007533 Published online by Cambridge University Press

$$x_2^{qs} = \frac{k_{001}^2 k_{200} A^2}{\omega_n^6}\left\{1+\frac{e^{-\sigma t}}{4\left(1-\zeta^2\right)^{3/2}}\left[4\omega_d t\mathrm{Cos}\left(\omega_d t+\varphi\right)-2(3-2\zeta^2)\mathrm{Sin}\left(\omega_d t+\varphi\right)\right.\right.$$
$$\left.-\mathrm{Sin}\left(\omega_d t+3\varphi\right)-\frac{1}{\sqrt{9-8\zeta^2}}\mathrm{Sin}\left(\omega_d t-2\varphi-\hat{\varphi}\right)\right] \quad \ldots (52)$$
$$\left.+\frac{e^{-2\sigma t}}{4\left(1-\zeta^2\right)}\left[2+\frac{1}{\sqrt{1-\zeta^2}}\mathrm{Sin}\left(2\omega_d t+3\varphi\right)\ -\frac{1}{\sqrt{1-\zeta^2}\sqrt{9-8\zeta^2}}\mathrm{Sin}\left(2\omega_d t+2\varphi+\hat{\varphi}\right)\right]\right\}$$

$$x_2^{bsr} = \frac{k_{001}^2 k_{110} A^2}{\omega_n^5}\frac{e^{-\sigma t}}{2\left(1-\zeta^2\right)^{3/2}\left(9-8\zeta^2\right)}\left\{\left[16\zeta\left(1-\zeta^2\right)^{3/2}-\left(9-8\zeta^2\right)(\omega_d t)\right]\ \mathrm{Cos}\left(\omega_d t\right)+\left[3-2\zeta^2\right]\mathrm{Sin}\left(\omega_d t\right)\right.$$
$$\left.+\sqrt{1-\zeta^2}e^{-\sigma t}\left[\left(3-4\zeta^2\right)\mathrm{Cos}\left(2\omega_d t+\varphi\right)+4\zeta\sqrt{1-\zeta^2}\mathrm{Sin}\left(2\omega_d t+\varphi\right)+\zeta\left(9-8\zeta^2\right)\right]\ \right\} \quad \ldots (53)$$

$$x_2^{qr} = \frac{k_{001}^2 k_{020} A^2}{4\omega_d^3\omega_n}\left\{e^{-2\sigma t}\left(2\mathrm{Sin}\left(\varphi\right)+\mathrm{Sin}\left(2\omega_d t+\varphi\right)-\frac{1}{\sqrt{9-8\zeta^2}}\mathrm{Sin}\left(2\omega_d t+\hat{\varphi}\right)\right)\right.$$
$$\left.+e^{-\sigma t}\left(2\mathrm{Sin}\left(\omega_d t-\varphi\right)-\mathrm{Sin}\left(\omega_d t+\varphi\right)-\frac{1}{\sqrt{9-8\zeta^2}}\mathrm{Sin}\left(2\omega_d t-\hat{\varphi}\right)\right)\right\} \quad \ldots (54)$$

$$x_2^{bsi} = \frac{k_{001}k_{101}A^2}{\omega_n^4}\left\{1-\frac{e^{-\sigma t}}{2\left(1-\varsigma^2\right)^{3/2}}\left[\varsigma\mathrm{Sin}\left(\omega_d t\right)+2\left(1-\varsigma^2\right)\mathrm{Sin}\left(\omega_d t+\varphi\right)-\omega_d t\mathrm{Cos}\left(\omega_d t+\varphi\right)\right]\right\} \quad \ldots (55)$$

$$x_2^{bri} = \frac{k_{001}k_{011}e^{-\tilde{\mathrm{N}}t}}{2\omega_d^3}\left\{\mathrm{Sin}\left(\omega_d t\right)-t\omega_d\mathrm{Cos}\left(\omega_d t\right)\right\} \quad \ldots (56)$$

$$x_2^{qi} = \frac{k_{002}A^2}{\omega_n^2}\left\{1-\frac{e^{-\sigma t}}{\sqrt{1-\varsigma^2}}\mathrm{Sin}\left(\omega_d t+\varphi\right)\right\} \quad \ldots (57)$$

Assembling the linear term x_1 along with the nonlinear components x_2^{qs}, x_2^{bsr}, x_2^{qr}, x_2^{bsi}, x_2^{bri} and x_2^{qi} and is the overall system response to a step input. Each term has different influences on the overall behaviour. Figures 19-24 show the generic shape of the each individual component in the case of $0 < \zeta < 1$. As in the case of the first order system, both linear and quadratic input terms have the same generic shape with different gain; $k_{001}A/\omega_n^2$ in the case of linear term and $k_{002}A^2/\omega_n^2$ in the case of quadratic input component.

All responses start at zero with a zero rate (initial condition), and head upward or downward depending on their equivalent signs. The nonlinear components x_2^{qx}, x_2^{bsr}, x_2^{qr}, x_2^{bsi} and x_2^{bri} have noticeable initial time lags. If a 2% tolerance is considered to define these lag vicinities, the equivalent time lags are computed as:

$$\tau_{rl}^{qs} = \frac{1\cdot 5\zeta - 0.05}{\sigma},\quad \tau_{rl}^{bsr} = \frac{1\cdot 33\zeta - 0\cdot 05}{\sigma},\quad \tau_{rl}^{qr} = \frac{0\cdot 38\zeta - 0\cdot 03}{\sigma}$$
$$\tau_{rl}^{bsi} = \frac{0\cdot 97\zeta - 0\cdot 02}{\sigma},\quad \tau_{rl}^{bri} = \frac{0\cdot 33\zeta - 0\cdot 02}{\sigma} \quad \ldots (58)$$

https://doi.org/10.1017/S0001924000007533 Published online by Cambridge University Press

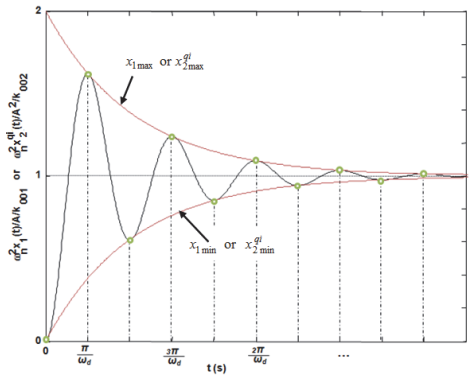


Figure 19. Second order system linear or quadratic input response to step input ($0 < \zeta < 1$).

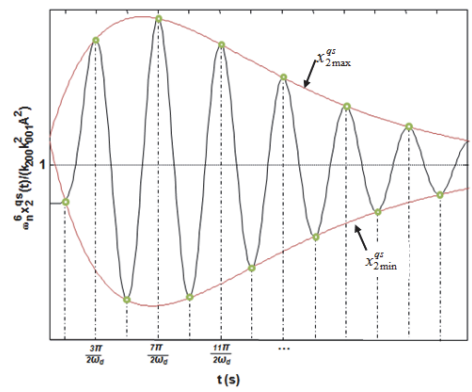


Figure 20. Second order system quadratic state response to step input ($0 < \zeta < 1$).

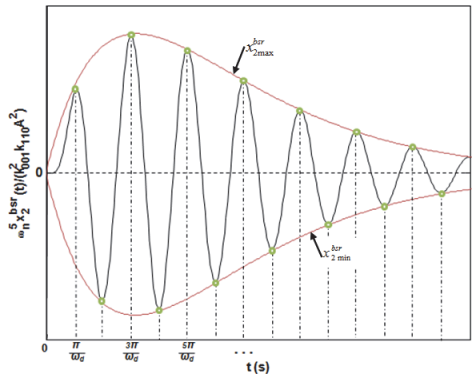


Figure 21. Second order system bilinear state-rate response to step input ($0 < \zeta < 1$).

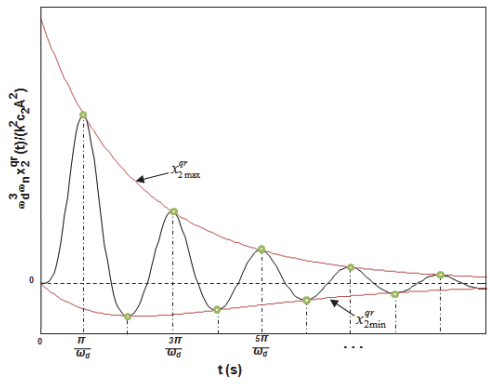


Figure 22. Second order system quadratic rate response to step input ($0 < \zeta < 1$).

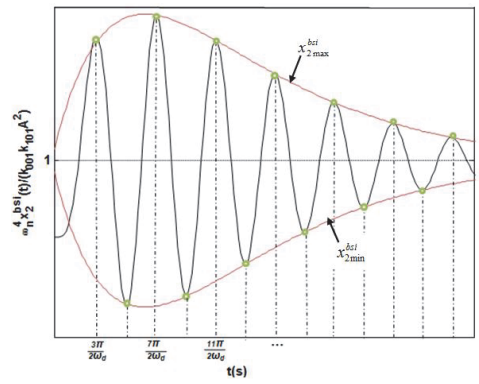


Figure 23. Second order system bilinear state-input response to step input ($0 < \zeta < 1$).

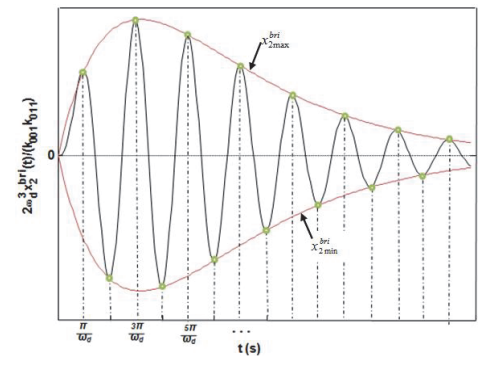


Figure 24. Second order system bilinear rate-input response to step input ($0 < \zeta < 1$).

https://doi.org/10.1017/S0001924000007533 Published online by Cambridge University Press

where τ_{r1}^{qs}, τ_{r1}^{bsr}, τ_{r1}^{qr}, τ_{r1}^{bst}, and τ_{r1}^{bri} are the time lags for x_2^{qx}, x_2^{bsr}, x_2^{qr}, x_2^{bsi} and x_2^{bri} respectively. Note that because of the expressions complexity of these nonlinear components, a fitting technique is employed to find approximate expressions for the equivalent time lags as listed in Equation (58). The 2% is defined by the steady value of each term in the case of x_{r1}^{qs}, $x_{r1}^{bsr}$and x_{r1}^{bsi}, while the 2% is defined by the maximum value in the case of x_{r1}^{qr} and x_{r1}^{bri}. The linear term and the quadratic input component do not have such time lags. Both immediately start to rise to their steady value. This observation is consistent with the one in the first order system case, which emphasises that any noticeable change in the initial slope, from that given by linear model, is traced back to the quadratic input nonlinearity. Also, the time lags are the instances at which a deviation between linear and nonlinear simulation starts to be significant in the case of a zero quadratic input coefficient.

Leaving the 2% vicinities, all responses oscillate around their equivalent steady values. All terms oscillate with the same frequency ω_d generating a set of maximum and minimum points. Both quadratic state x_2^{qs} and bilinear state-input x_2^{bsi} components achieve their minimum and maximum values at the same times, which are $(4n+5)\pi/2/\omega_d$ and $(4n+3)\pi/2/\omega_d$ respectively, where $n = 0,1,2,\ldots$ The rest of the other components consistent with the linear term have minimum and maximum values at times $(2n+3)\pi/\omega_d$ and $2(n+1)\pi/\omega_d$, where $n = 0,1,2,\ldots$ Based on these results, both quadratic state x_2^{qs} and bilinear state-input components produce a phase shift in the observed peaks, especially after the linear behaviour settles down. As shown in Fig. 22, the quadratic rate component does not symmetrically oscillate around zero, which means that the total response experiences a non-symmetric oscillatory response in the presence of a significant quadratic rate nonlinearity.

The loci of the maximum and minimum points are achieved by substituting their equivalent time values in the original expressions as:

$$x_{1\min} = \frac{k_{001}A}{\omega_n^2}\left\{1-\frac{e^{-\sigma t}}{\sqrt{1-\zeta^2}}\right\} \quad , \quad x_{1\max} = \frac{k_{001}A}{\omega_n^2}\left\{1+\frac{e^{-\sigma t}}{\sqrt{1-\zeta^2}}\right\} \qquad \ldots (59)$$

$$x_{2\min}^{qs} = \frac{k_{001}^2 k_{200}A^2}{\omega_n^6}\left\{1-\psi_7(\zeta)e^{-\sigma t}+\psi_8(\zeta)e^{-2\sigma t}\right\}, \quad x_{2\max}^{qs} = \frac{k_{001}^2 k_{200}A^2}{\omega_n^6}\left\{1+\psi_7(\zeta)e^{-\sigma t}+\psi_8(\zeta)e^{-2\sigma t}\right\}$$

$$\psi_7 = \frac{1}{4\left(1-\zeta^2\right)^{3/2}}\left[4\omega_d \mathrm{Sin}(\varphi)+2(3-2\zeta^2)\mathrm{Cos}(\varphi)+\mathrm{Cos}(3\varphi)+\frac{1}{\sqrt{9-8\zeta^2}}\mathrm{Cos}(2\varphi+\hat{\varphi})\right] \qquad \ldots (60)$$

$$\psi_8 = \frac{1}{4\left(1-\zeta^2\right)}\left[2-\frac{1}{\sqrt{1-\zeta^2}}\mathrm{Sin}(3\varphi)+\frac{1}{\sqrt{1-\zeta^2}\sqrt{9-8\zeta^2}}\mathrm{Sin}(2\varphi+\varphi)\right]$$

$$x_{2\min}^{bsr} = \frac{k_{001}^2 k_{110}A^2}{\omega_n^5}\left\{\frac{-\omega_d t e^{-\sigma t}}{2\left(1-\zeta^2\right)^{3/2}}+\frac{8\zeta}{9-8\zeta^2}\left(e^{-2\sigma t}-e^{-\sigma t}\right)\right\}$$

$$x_{2\max}^{psr} = \frac{k_{001}^2 k_{110}A^2}{\omega_n^5}\left\{\frac{\omega_d t e^{-\sigma t}\left(9+8\zeta^2\right)}{2\left(1-\zeta^2\right)^{3/2}\left(9-8\zeta^2\right)}-\frac{8\zeta}{9-8\zeta^2}\left(e^{-2\sigma t}-e^{-\sigma t}\right)\right\} \qquad \ldots (61)$$

$$x_{2\min}^{qr} = \frac{3\left(4-9\zeta^2+4\zeta^4\right)\ k^2c_2A^2}{2\omega_d^4\left(9-8\zeta^2\right)}\left(e^{-2\sigma t}-e^{-\sigma t}\right), \quad x_{2\max}^{qr} = \frac{3\left(4-9\zeta^2+4\zeta^4\right)\ k^2c_2A^2}{2\omega_d^4\left(9-8\zeta^2\right)}\left(e^{-2\sigma t}+e^{-\sigma t}\right). \qquad \ldots (62)$$

https://doi.org/10.1017/S0001924000007533 Published online by Cambridge University Press

$$x_{2\min}^{bsi} = \frac{k_{001}k_{101}A^2}{\omega_n^4}\left\{1-\frac{e^{-\sigma t}}{2\left(1-\varsigma^2\right)^{3/2}}\left[\varsigma\left(3-2\varsigma^2\right)+\omega_d t\sqrt{1-\varsigma^2}\right]\right\}$$
$$x_{2\max}^{bsi} = \frac{k_{001}k_{101}A^2}{\omega_n^4}\left\{1+\frac{e^{-\sigma t}}{2\left(1-\varsigma^2\right)^{3/2}}\left[\varsigma\left(3-2\varsigma^2\right)+\omega_d t\sqrt{1-\varsigma^2}\right]\right\} \quad \ldots (63)$$

$$x_{2\min}^{bri} = \frac{-k_{001}k_{011}A^2}{2\omega_d^3}\left\{t\omega_d e^{-\sigma t}\right\},\quad x_{2\max}^{bri} = \frac{k_{001}k_{011}A^2}{2\omega_d^3}\left\{t\omega_d e^{-\sigma t}\right\} \quad \ldots (64)$$

$$x_{2\max}^{qi} = \frac{k_{002}A^2}{\omega_n^2}\left\{1-\frac{e^{-\sigma t}}{\sqrt{1-\zeta^2}}\right\},\ x_{2\min}^{qi} = \frac{k_{002}A^2}{\omega_n^2}\left\{1+\frac{e^{-\sigma t}}{\sqrt{1-\zeta^2}}\right\} \quad \ldots (65)$$

where x^i_{jmin} and x^i_{jmax} are the loci of minimum and maximum points of the term x^i_j, where $i = \{(), qs, bsr, qr, bsi, bri, qi\}$ and $j = \{1, 2\}$. These loci are good estimators for the settling time of each component. For the linear term and quadratic input component, the response settling time based on their equivalent loci is $\tau^1_{rs} = \tau^{qi}_{rs} = 4/\sigma$. By solving a quadratic equation from equating Equation (62) to a 2% value, the settling time of the quadratic rate component is

$$\tau_{rs}^{qr} = \frac{1}{\sigma}\ln\left\{\frac{2}{-1+\sqrt{1+0\cdot08/\psi_9(\zeta)}}\right\} \text{ and } \psi_9(\zeta) = \frac{6\left(4-9\zeta^2+4\zeta^4\right)}{\left(9-8\zeta^2\right)} \quad \ldots (66)$$

For the rest of components x_2^{qs}, x_2^{bsr}, x_2^{bsi} and x_2^{bri} a fitting technique is to compute the settling times as

$$\tau_{rs}^{qs} = \frac{6\cdot8\zeta^2-8\cdot2\zeta+9\cdot0}{\sigma},\ \tau_{rs}^{bsr} = \frac{-0\cdot23\zeta^2-0\cdot54\zeta+6\cdot8}{\sigma}$$
$$\tau_{rs}^{bsi} = \frac{7\cdot4\zeta^2-8\cdot3\zeta+8\cdot2}{\sigma},\ \tau_{rs}^{bri} = \frac{-2\cdot2\zeta^2-2\cdot7\zeta+7\cdot4}{\sigma} \quad \ldots (67)$$

The resultant settling times of these components have more damping sensitivity than the linear term. The overall settling time depends on the ratio between the coefficients, undamped natural frequency, and damping ratio. If the system has low frequency, the nonlinearity of the system starts to be significant even if the system has low nonlinear coefficients but the influence of this frequency on the settling time is the same as in the linear case. On the other hand, the damping ratio ζ does not change the ratio between the linear and nonlinear terms, but changes the overall settling time. In addition, the sign ratio between the coefficients plays an important role in the settling time. Negative nonlinear coefficients may lead to improve the settling time or make it longer.

The bilinear state-rate, quadratic rate, and bilinear rate-input components oscillate around a zero value. This observation indicates that the bilinear position-rate and quadratic rate components have no influence on the overall response's steady value. Thus, for a stable case $\zeta > 0$, when the total system behaviour starts to settle down, its rate settles at zero ($v = v_1 + v_2 + \ldots \approx 0$) and theses components diminish. Linear, quadratic state, bilinear state-input, and quadratic input components, on the other hand, oscillate around non-zero values, which means that they have influences on the

https://doi.org/10.1017/S0001924000007533 Published online by Cambridge University Press

steady value for the step input case. Using this assembly, the estimated overall steady value x_{ss} is

$$x_{ss} = \frac{k_{001}A}{\omega_n^2} + \frac{k_{001}^2 k_{200}A^2}{\omega_n^6} + \frac{k_{001}k_{101}A^2}{\omega_n^4} + \frac{k_{002}A^2}{\omega_n^2} \quad \ldots (68)$$

The linear theory provides $\frac{x_{ss}}{A} = \frac{k_{001}}{\omega_n^2}$, is a function of the system' parameters only. The nonlinear Volterra-based estimation in Equation (68) shows $\frac{x_{ss}}{A}$ is a function of the system's parameters and input's amplitude.

Adding all the results for the second order SDOF system with the first order SDOF system illustrates how many nonlinear characteristics appearing in aircraft can influence the dynamic behaviour. These characteristics are not accessible from the linear analysis. The analysis has been applied for first and second order systems, which are the foundation for rendering the generic aircraft behaviour. To judge the efficiency and the worth of this analysis, the results are applied to a set of uniaxial flight motions in the following section.

Increasing the input amplitude or the strength of the nonlinearity also increases the error between the developed Volterra model and the exact solution. More Volterra terms are then required, which leads to a more complicated solution. In order to avoid such an input amplitude-accuracy or nonlinearity strength-accuracy dependency, the authors have developed the piecewise Volterra kernel approach in Ref. 28 and Volterra parameter varying (VPV) approach in Ref. 28 to break down the entire region into a set of sub-regions, and interpolation is then employed to move between these sub-regions. Each sub-region has an operating range of the input amplitude within a specific error tolerance. For example in Ref. 28, an approximate global two-term Volterra model was developed for the nonlinear short-period motion through four sub-regions. Each sub-region has an operating-elevator deflection range (input signal). The first and second kernels are then defined each as a function of the operating elevator deflection. Instead, if a traditional Volterra approach were used, nine kernels (nine-dimensional convolution integration or 18 states in case of the PLTI) would then be required to capture the system behaviour. Based on this piecewise approach, the developed two-term Volterra model was able to capture limit cycling behaviour for the stall and post-stall regions.

8.0 LOW ORDER MOTION EXAMPLES

In this Section, numerical examples of surge and pitch motions are presented to show the capability of the developed Volterra-based model to understand and predict aircraft behaviour. For each motion, the trim values of the total nonlinear aircraft model are computed at certain operating conditions. The low order flight systems are then extracted from the overall model. These low order systems still have the aerodynamic-propulsive coefficients represented by look-up tables. After that, the finite difference technique generates both first and second order stability and control derivatives around the previously considered operating conditions. These derivatives are passed to linear-based and Volterra-based models, while the look-up tables are used for the nonlinear simulation.

In the surge motion example, consider the aircraft flies levelly at $\hat{\theta}$ $[H_o\ V_o]^T = [10(\text{kft})\ 300(\text{ft/s})]^T$. The required angle-of-attack and elevator deflection to lift the aircraft and balance the pitching moment are $\alpha_o = 15{\cdot}85\text{deg}$ and $\delta_{eo} = -11{\cdot}07\text{deg}$, while the required thrust is generated by adjusting the throttle deflection to $\delta_{tho} = 28\%$. Recall Equation (7) and use the finite difference to calculate the derivatives at this flight condition, the equivalent surge equation of motion is

https://doi.org/10.1017/S0001924000007533 Published online by Cambridge University Press

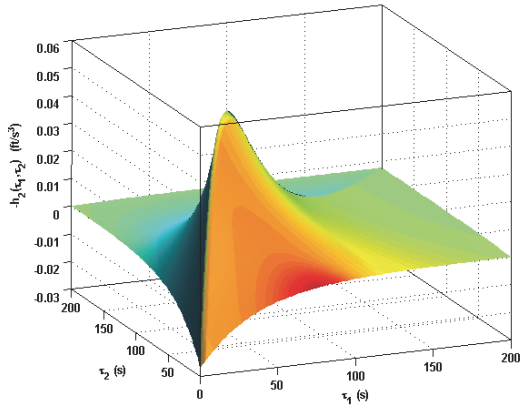


Figure 25. Surge motion second kernel at H_o = 10kft and V_o = 300ft/s.

$$\Delta\dot{V} = \underbrace{-0\cdot0285}_{a=k_{10}}\Delta V + \underbrace{13\cdot44}_{k_{01}}\Delta\delta_{th} \underbrace{-4\cdot57\times10^{-5}}_{k_{20}}\Delta V^2 + \underbrace{4\cdot06\times10^{-3}}_{k_{11}}\Delta V\Delta\delta_{th} \qquad \ldots (69)$$

In Equation (69), the quadratic throttle deflection is zero (k_{02} = 0) for the current aircraft model. Based on Equation (6), the parameters of the Volterra-based model in Equation (69) can be expressed in terms of the linear and nonlinear stability and control derivatives as

$$\begin{aligned} k_{10} &= \frac{\mathrm{Cos}(\alpha_o)}{m}\frac{\partial T}{\partial V} - \frac{2\rho S V_o}{m} C_D(\alpha_o,\delta_{eo}) & k_{01} &= \frac{\mathrm{Cos}(\alpha_o)}{m}\frac{\partial T}{\partial \delta_{th}} \\ k_{20} &= \frac{\mathrm{Cos}(\alpha_o)}{2m}\frac{\partial^2 T}{\partial V^2} - \frac{\rho S}{m} C_D(\alpha_o,\delta_{eo}) & k_{11} &= \frac{\mathrm{Cos}(\alpha_o)}{m}\frac{\partial^2 T}{\partial V\partial \delta_{th}} \end{aligned} \qquad \ldots (70)$$

The surge motion's first kernel is an exponential function starting at k_{01} = 13·44 and heads downward with an angle φ = Arctan(a) = 1·6 deg reaching zero at time infinity. The required time to settle this first kernel inside a 2% band is $\tau_{ks}^1 = 4/|a|$ = 140·4s. (see Equation (31)). The surge motion's second kernel has two components: quadratic velocity component h_2^{qs} and bilinear velocity-throttle component h_2^{bsi}. The linear term a (k_{10} = –0·0285 1/s) has a relatively low value indicating that the quadratic component h_2^{qs} is more dominant than the bilinear component h_2^{bsi} according to Equation (29). This fact makes the shape of the second kernel look close to the quadratic state kernel shape in Fig. 4. Adding the two components together leads to the overall shape of the second kernel as shown in Fig. 25. The developed first and second kernels of the surge motion can then be used to predict the system behaviour to any throttle deflection.

Considering the step response more specifically, using the results of the developed step response in Section VI, the lag time of each nonlinear component is $\tau_{r1}^{qs} = 0{\cdot}45/|a|$ = 15s and $\tau_{r1}^{bsi} = 0{\cdot}2/|a|$ = 7s. The linear term has a settling time $4/|a|$ = 140·4s, while $\tau_{rs}^{qs} = 6{\cdot}6/|a|$ = 231·6s and $\tau_{rs}^{bsi} = 5{\cdot}8/|a|$ = 203·5s. Based on Equation (49), the steady value as a function of input's amplitude is ΔV_{ss} = $471{\cdot}6\Delta\delta_{th} - 289{\cdot}5\Delta\delta_{th}^2$ft/s.

For example, assume an input excitation $\Delta\delta_{th}$ =15%. Figure 26 shows the response of each nonlinear component and the overall estimated response is shown in Fig. 27. At time t = 15s, the linear model deviates from the nonlinear one. This deviation time is the quadratic time lag. The linear-based model has a steady value $V_{ss}^{linear} = 300 + 471{\cdot}6\Delta\delta_{th}|_{0{\cdot}15}$ = 371ft/s, while $V_{ss}^{Volterra}$ = 300

https://doi.org/10.1017/S0001924000007533 Published online by Cambridge University Press

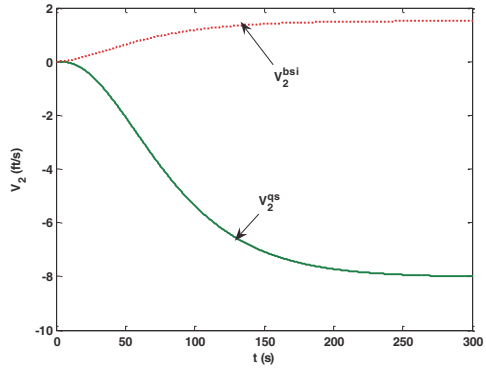


Figure 26. Surge motion nonlinear step response components for Δδth = 15%.

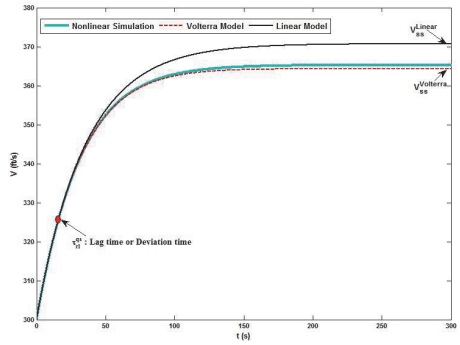


Figure 27. Surge motion step response for Δδth = 15%.

$+ 471{\cdot}6\Delta\delta_{th} - 289{\cdot}5\Delta\delta_{th}^2|_{0{\cdot}15} = 364{\cdot}3$ft/s. The nonlinear simulation has a steady value 365ft/s. This result shows how the quadratic component has a significant influence on the steady value. The quadratic component in this model represents the second derivative of the X-axis total force with velocity, which is the drag and thrust variation with the velocity squared. The required time to achieve the steady values in the case of the linear is $\tau_{rs}^{linear} = 4/|a| = 140$s, while $\tau_{rs}^{Volterra} = 114$s. The nonlinear simulation has a total settling time 118s, which is much less than the linear settling time because of the negative sign of the quadratic position component.

The second example represents the pitch motion at an altitude $H_o = 40$kft and total velocity $V_o = 530$ft/s. For a rectilinear motion, the computed trimming variables are $\theta_o = \alpha_o = 15{\cdot}6$deg, $\delta_{eo} = -2{\cdot}6$deg, and $\delta_{tho} = 98{\cdot}8\%$. Using the finite difference technique, the reduced pitch equations of motion, equivalent to Equation (9), are:

$$\Delta\dot{\theta} = \Delta q$$
$$\Delta\dot{q} = \underbrace{-0{\cdot}79}_{k_{100}}\Delta\theta \underbrace{-0{\cdot}36}_{k_{010}}\Delta q \underbrace{-3{\cdot}15}_{k_{001}}\Delta\delta_e + \underbrace{1{\cdot}05}_{k_{200}}\Delta\theta^2 + \underbrace{0{\cdot}16}_{k_{110}}\Delta\theta\Delta q + \underbrace{0{\cdot}29}_{k_{101}}\Delta\theta\Delta\delta_e \underbrace{-0{\cdot}0014}_{k_{002}}\Delta\delta_e^2 \quad \ldots (71)$$

In Equation (71), the quadratic rate coefficient $k_{020} = 0$ and the bilinear rate-input coefficient $k_{011} = 0$. Thus, both plunge force and pitch moment coefficients are linear related to the pitch rate q with a zero correlation to the elevator deflection δ_e. The pitch motion model has a damping ratio $\zeta = 0{\cdot}2$, damping factor $\sigma = 0{\cdot}18$ 1/s, undamped natural frequency $\omega_n = 0{\cdot}89$ rad/s, and damped natural frequency $\omega_d = 0{\cdot}87$ rad/s. The parameters of the Volterra-based model can be traced back to the linear and nonlinear stability and control derivatives by comparing Equation (71) by Equation (8). This leads to:

$$k_{100} = \frac{\bar{q}S\bar{c}}{I_Y}\frac{\partial C_m}{\partial\alpha} \qquad k_{010} = \frac{\bar{q}S\bar{c}^2}{2I_YV_0}C_{m_q} \qquad k_{001} = \frac{\bar{q}S\bar{c}}{I_Y}\frac{\partial C_m}{\partial\delta_e} \qquad k_{200} = \frac{\bar{q}S\bar{c}}{2I_Y}\frac{\partial^2 C_m}{\partial\alpha^2}$$
$$k_{110} = \frac{\bar{q}S\bar{c}^2}{2I_YV_0}\frac{\partial C_{m_q}}{\partial\alpha} \qquad k_{101} = \frac{\bar{q}S\bar{c}}{I_Y}\frac{\partial^2 C_m}{\partial\alpha\partial\delta_e} \qquad k_{002} = \frac{\bar{q}S\bar{c}}{2I_Y}\frac{\partial^2 C_m}{\partial\delta_e^2} \quad \ldots (72)$$

The first kernel starts at zero with a negative slope and keeps oscillating around a zero value with a frequency $\omega_d = 0{\cdot}87$ rad/s. The amplitude of this oscillation decreases with time and settles inside a 2% band of the gain $|k_{001}/\omega_n| = 3{\cdot}45$ at time $\tau_{ks}^1 = 4/|\sigma| \; 22{\cdot}2$s. The second kernel has four

https://doi.org/10.1017/S0001924000007533 Published online by Cambridge University Press

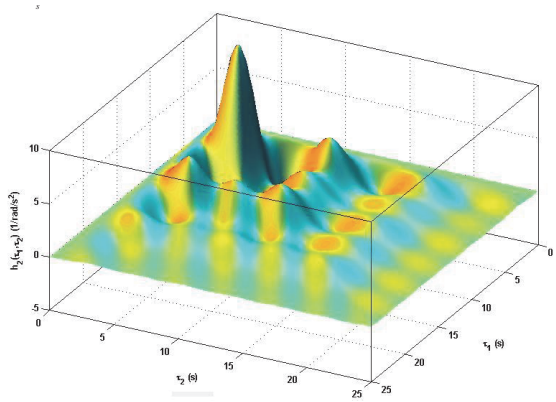


Figure 28. Pitch motion second kernel at H_o = 40kft and V_o = 530ft/s.

components. Based on Equations (34)-(39), the influence of each component on the total second kernel, from highest to lowest, is: quadratic state component h_2^{qs} (with a weight $k_{200}k_{001}^2/2\omega_d^4 = 6{\cdot}86$), bilinear state-rate component h_2^{bsr} (with a weight $k_{110}k_{001}^2/2\omega_d^3\sqrt{1-\zeta^2} = 1{\cdot}18$), bilinear state-input component h_2^{bsi} (with a weight $k_{101}k_{001}/2\omega_d^2 == -0{\cdot}59$), and quadratic input component h_2^{qi} (with a weight $k_{002}/\omega_d = -0{\cdot}0016$). Although the nonlinear coefficients in Equation (71) are in the same range, the analysis based on Volterra model shows that some nonlinearities dominate the others because of the operating frequency and damping ratio. The contribution of the quadratic input term is almost zero and can be removed from the model. Since the quadratic state component has the highest weight with a big difference compared to the other components, the total second kernel is expected to be close in shape to the quadratic state component h_2^{qs}. Figure 28 shows the total second kernel. The individual settling time of each component is $\tau_{ks}^{qs} = 19{\cdot}47$s, $\tau_{ks}^{bpr} = 19{\cdot}34$s, and $\tau_{ks}^{bsi} = \tau_{ks}^{qi} = 22{\cdot}23$s. Since the quadratic state component is dominant, the expected overall settling time is roughly close to $\tau_{ks}^{total} \approx 19{\cdot}47$s.

The developed first and second kernels of the pitch motion provide the seeking structural to predict and understand the system behaviour to any input. The step response analysis in Section VI is now recalled and used. The step response of each component can be specified by the following characteristics:

1. Time lags of each component in Equation (58) as $\tau_{r1}^{qs} = 1{\cdot}41$s, $\tau_{r1}^{bpr} = 1.22$ s, $\tau_{r1}^{bsi} = 0{\cdot}98$s and $\tau_{r1}^{qi} = 0$s.
2. Settling times in Equation (64) as $\tau_{rs}^{qs} = 41{\cdot}9$s, $\tau_{rs}^{bpr} = 37{\cdot}1$s, $\tau_{rs}^{bsi} = 37{\cdot}9$s and $\tau_{rs}^{qi} = 22{\cdot}2$s.
3. Steady values in Equation (68) as $\theta_{ss}^{qs} = 22{\cdot}06\Delta\delta_e^2$ rad, $\theta_{ss}^{bpr} = 0\Delta\delta_e^2$ rad, $\theta_{ss}^{bsi} = -1{\cdot}44\Delta\delta_e^2$ rad and $\theta_{ss}^{qi} = -0{\cdot}0017\Delta\delta_e^2$ rad, where $\Delta\delta_e$ is in rad.

The linear response, on the other hand, has a settling time $\tau_{rs}^{1} = 22{\cdot}2$s and a steady value $\theta_{rs}^{1} = -3{\cdot}98\,\Delta\delta_e$ rad. As a test case, the response of each nonlinear component is shown in Fig. 29 for an input of $\Delta\delta_e = 0{\cdot}75$deg. Figure 30 shows the result of assembling the linear term to the nonlinear components in a comparison with the linear response, while the nonlinear simulation is the benchmark. The three responses (Linear, Volterra, and Nonlinear) start at the value 15·5deg (trimming value) heading downward. The linear model deviates from both the nonlinear simulation and Volterra-based model at $t \approx 1{\cdot}5$s (almost equals to τ_{r1}^{qs}), when the nonlinear components start to be energetic.

https://doi.org/10.1017/S0001924000007533 Published online by Cambridge University Press

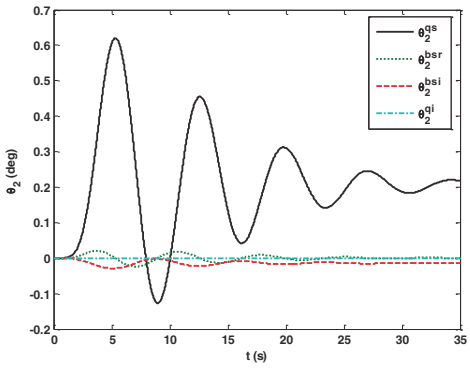


Figure 29. Pitch motion nonlinear step response components for $\Delta\delta_e$ = 0·75deg.

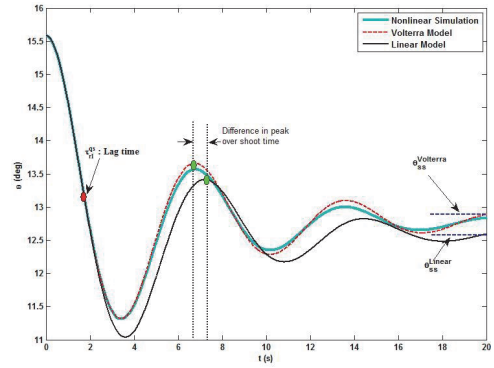


Figure 30. Pitch motion step response for $\Delta\delta_e$ = 0·75deg.

There is a difference in the times of the peak overshoot and undershoot between linear and nonlinear simulation. Based on Volterra model, this difference in times traces back to x_2^{qs} and x_2^{bsi} components, which head $\Delta t = \pi/2/\omega_d$ = 1·8s from the linear simulation. Volterra model with the nonlinear simulation consistently provides the times of the first two overshoot peaks at: 6·76s and 13·67s. The linear model, on the other hand, provides these times at: 7·22s and 14·43s. The developed analytical Volterra model not only proves the capability to render the transient response but also the steady response as $\theta_{ss}^{Volterra} = -3{\cdot}98\Delta\delta_e + 22{\cdot}06\Delta\delta_e^2 - 1{\cdot}44\Delta\delta_e^2 - 0{\cdot}0017\Delta\delta_e^2|_{\Delta\delta_e - 0{\cdot}75\text{deg}}$ = 12·79deg compared to θ_{ss}^{linear} 12·6deg from the linear model with an error 7%. The estimated settling time to reach this value is t_s^{linear} = 19·4s and t_s^{linear} = 24·6s.

9.0 CONCLUSION

A procedure to analytically assemble the constituents of the dynamic response of simple low order nonlinear systems based on multi-dimensional convolution expansion theory has been offered. The procedure provides closed-form expressions for the convolution integral kernels, which in turn lead to expressions for the time response for a step input. The explicit nature of the relational expressions allow cause-and-effect insights between nonlinearities present in the state space model and corresponding response traits. The procedure facilitates system prediction before employing computer simulation and/or system analysis after computer simulation. At this point in time, the procedure has only been developed for first and second order single degree of freedom systems. Expanding this framework to multi-axis motions is of future interest. Application to single state and dual state uni-axis aircraft motion exposed the source of differences between nonlinear and linear responses, specifically initial departure time, maximum and steady offsets differences in settling times, and oscillation frequency and phasing shifts.

ACKNOWLEDGEMENT

The first author would like to acknowledge that the presented work in this paper does not belong or represent his current affiliation, CNH-Fiat Industrial, at any level.

https://doi.org/10.1017/S0001924000007533 Published online by Cambridge University Press

REFERENCES

1. LIEBST, S. and NOLAN, C. A simplified wing rock prediction method, August 1993, AIAA-1993-3662, Atmospheric Flight Mechanic Conference, Monterey, CA, USA.
2. JAHNKE, C. and CULICK, C. Application of bifurcation theory to the high-angle-of-attack dynamics of the F-14, *AIAA J Aircr*, January-February 1994, **31**, (1), pp 26-34.
3. ANANTHKRISHNAN, N. and SUDHAKAR, K. Characterization of periodic motions in aircraft lateral dynamics, *AIAA J Guidance, Control, and Dynamics*, May-June 1996, **19**, (3), pp 680-685.
4. NANDAN , S. Applications of bifurcation methods to F-18 HARV open-loop dynamics in landing configuration, *Defense Science J*, April 2002, **52**, (2), pp 103-115.
5. GO, T. and RAMNATH, R. Analytical theory of three-degree-of-freedom aircraft wing rock, *AIAA J Guidance, Control, and Dynamics*, July-August 2004, **27**, (4), pp 657-664.
6. RICHARDSON, S. and LOWENBERG, M. A continuation design framework for nonlinear flight control problems, *Aeronaut J*, February 2006, **110**, (1104), pp 85-89.
7. SANCHEZ, G. Dynamics and control of single-line kites, *Aeronaut J*, 2006, **110**, (1111), pp 615-621.
8. RAGHAVENDRA, P., SAHAI, T., KUMAR, P., CHAUHAN, M. and ANANTHKRISHNAN, N. Aircraft spin recovery, with and without thrust vectoring, using nonlinear dynamic inversion, *AIAA J Aircr*, November-December 2005, **42**, (6), pp 1492-1503.
9. MEHRA, K., WOBURN, M., PRASANTH, K. and WOBURN, M. Bifurcation and limit cycle analysis of nonlinear pilot induced oscillations, August 1998, AIAA Atmospheric Flight Mechanics Conference, Boston, MA, USA.
10 NEWMAN, B. Dynamics and control of limit cycling motions in boosting rockets, *AIAA J Guidance, Control, and Dynamics*, March-April 1995, **18**, (2), pp 280-286.
11 DUDA, H. Effects of rate limiting elements in flight control systems a new PIO-criterion, August 1995, AIAA Guidance, Navigation and Control Conference, Baltimore, MD, USA.
12 KLYDE, H., MCRUER, T. and MYERS, T. PIO analysis with actuator rate limiting, July 1996, AIAA Atmospheric Flight Mechanics Conference, San Diego, CA, USA.
13 GO, T. Lateral-Directional aircraft dynamics under static moment nonlinearity, *AIAA J Guidance, Control, and Dynamics*, January–February 2009, **32**, (1), pp 305-309.
14 MEHRA, K., WASHBURN, B. and CARROL, V. A study of the application of singular perturbation theory, 1979, NASA CR-3167.
15 NAIDU, D. and CALISE, A. Singular perturbations and time scales in guidance and control of aerospace systems: a survey, *AIAA J Guidance, Control, and Dynamics*, 2001, **24**, (6), pp 1057-1078.
16 RAGHAVAN, B. and ANANTHKRISHNAN, N. Small perturbation analysis of airplane dynamics with dynamic stability derivatives redefined, August 2005, AIAA Atmospheric Flight Mechanic Conference, San Francisco, CA, USA.
17 MEASE, K., BHARADWAJ, S. and IRAVANCHY, S. Timescale analysis for nonlinear dynamical systems, *AIAA J Guidance, Control, and Dynamics*, 2003, **26**, (2), pp 318-330.
18 DESAI, P. and CONWAY, B. Two timescale discretization scheme for collocation, *AIAA J Guidance, Control, and Dynamics*, 2008, **31**, (5), pp 1316-1322.
19 VOLTERRA, V. *Theory of Functionals and of Integral and Integro-Differential Equations*, 1958, Dover, New York, USA.
20 RUGH, J. W. *Nonlinear System Theory: The Volterra/Wiener Approach*, 1981, John Hopkins University Press.
21 WIENER, N. Response of a nonlinear device noise, 1942, Technical Report No 165, Massachusetts Institute of Technology Radiation Laboratory, Cambridge, MA, USA.
22 BRILLIANT, M. Theory of the analysis of nonlinear systems, 1958, Technical Report No 345, Massachusetts Institute of Technology Radiation Laboratory, Cambridge, MA, USA.
23 GEORGE, D. Continuous nonlinear systems, 1959, Technical Report No 355, Massachusetts Institute of Technology Radiation Laboratory.
24 MOHLER, R. R. Nonlinear stability and control study of highly maneuverable high performance aircraft, 1991, NASAOSU-ECE Report No 91-01.
25 STALFORD, H., BAUMANN, W., GARRETT, E. F. and HERMAN, T. Accurate modeling of nonlinear system using volterra series submodels, July 1987, ACC American Control Conference, pp 886-891, Minneapolis, MN, USA.
26 SUCHOMEL, C. F. Nonlinear flying qualities — one approach, January 1987, AIAA Aerospace Sciences Meeting, Reno, NV, USA.

https://doi.org/10.1017/S0001924000007533 Published online by Cambridge University Press

27 OMRAN, A. and NEWMAN, B. Full envelope nonlinear parameter-varying model approach for atmospheric flight dynamics, *AIAA J Guidance, Control, and Dynamics*, January-February 2012, **35**, (1), pp 270-283.
28 OMRAN, A. and NEWMAN, B. Piecewise global Volterra nonlinear modeling and characterization for aircraft dynamics, *AAIJ J Guidance, Control, and Dynamics*, May-June 2009, **32**, (3), pp 749-759.
29. NGUYEN, L., OGBURN, M., GILBERT, W., KIBLER, K., BROWN, P. and DEAL, P. Simulator study of stall/post-stall characteristics of a fighter airplane with relaxed longitudinal static stability, 1979, NASA TP-1538.
30. STEVENS, B. and LEWIS, F. *Aircraft Control and Simulation*, 1992, John Wiley & Sons, New York, USA.
31. FRANZ, M. and SCHOLKOPF, B. A unifying view of Wiener and Volterra theory and polynomial kernel regression, *Neural Computation*, December 2006, **18**, (12), pp 3097-3118.
32. GILBERT, E. Functional expansions for the response of nonlinear differential systems, *IEEE Transactions on Automatic Control*, December 1977, **22**, (6), pp 909-921.
33. NGUYEN, T., WHIPPLE, D. and BRANDON, J. Recent experience of unsteady aerodynamic effect on flight dynamics at high angle of attack, May 1985, AGARD Conference Proceedings, Symposium on Unsteady Aerodynamics-Fundamentals and Applications to Aircraft Dynamics, Gottingen, Germany.
34. OMRAN, A. and NEWMAN, B. Analytical nonlinear analysis methodology for reduced aircraft dynamical systems, 2010, ICAS 2010 Annual International Council of the Aeronautical Sciences Conference, 19-24 September 2010, Nice, France.
35. OMRAN, A. and NEWMAN, B. On dynamical assembly of nonlinear uniaxial atmospheric flight mechanics, 10-13 August 2009, AIAA Atmospheric Flight Mechanics Conference and Exhibition, Chicago, IL, USA.
36. ZILL, D., WRIGHT, W. and CULLEN, M. *Advanced Engineering Mathematics*, 2011, Jones & Bartlett Learning.

https://doi.org/10.1017/S0001924000007533 Published online by Cambridge University Press